Exploring the faint young Sun problem and the possible climates of the Archean Earth with a 3-D GCM

B. Charnay, F. Forget, R. Wordsworth, J. Leconte, E. Millour, F. Codron, A. Spiga

Exploring the faint young Sun problem and the possible climates of the Archean Earth with a 3-D GCM

B. Charnay,[1] F. Forget,[1] R. Wordsworth,[2] J. Leconte,[1] E. Millour,[1]
F. Codron,[1] and A. Spiga[1]

Received 18 May 2013; revised 9 August 2013; accepted 4 September 2013; published 19 September 2013.

[1] Different solutions have been proposed to solve the "faint young Sun problem," defined by the fact that the Earth was not fully frozen during the Archean despite the fainter Sun. Most previous studies were performed with simple 1-D radiative convective models and did not account well for the clouds and ice-albedo feedback or the atmospheric and oceanic transport of energy. We apply a global climate model (GCM) to test the different solutions to the faint young Sun problem. We explore the effect of greenhouse gases (CO_2 and CH_4), atmospheric pressure, cloud droplet size, land distribution, and Earth's rotation rate. We show that neglecting organic haze, 100 mbar of CO_2 with 2 mbar of CH_4 at 3.8 Ga and 10 mbar of CO_2 with 2 mbar of CH_4 at 2.5 Ga allow a temperate climate (mean surface temperature between 10°C and 20°C). Such amounts of greenhouse gases remain consistent with the geological data. Removing continents produces a warming lower than +4°C. The effect of rotation rate is even more limited. Larger droplets (radii of 17 μm versus 12 μm) and a doubling of the atmospheric pressure produce a similar warming of around +7°C. In our model, ice-free water belts can be maintained up to 25°N/S with less than 1 mbar of CO_2 and no methane. An interesting cloud feedback appears above cold oceans, stopping the glaciation. Such a resistance against full glaciation tends to strongly mitigate the faint young Sun problem.

Citation: Charnay, B., F. Forget, R. Wordsworth, J. Leconte, E. Millour, F. Codron, and A. Spiga (2013), Exploring the faint young Sun problem and the possible climates of the Archean Earth with a 3-D GCM, *J. Geophys. Res. Atmos.*, *118*, 10,414–10,431, doi:10.1002/jgrd.50808.

1. Introduction and Background

1.1. The Faint Young Sun Problem

[2] The Archean is the geological era following the Hadean (starting with Earth formation 4.56 Ga) and preceding the Proterozoic. It starts at 3.8 Ga, after the Late Heavy Bombardment (LHB), and ends at 2.5 Ga with the Great Oxidation Event. The first reported fossils of bacteria date back 3.5 Ga [*Schopf*, 2006] and there is possibly evidence for life from carbon isotopes up to 3.8 Ga [*Mojzsis et al.*, 1996; *Rosing*, 1999]. The emergence of life is believed to have occurred before 3.5 Ga and maybe even before the LHB [*Nisbet and Sleep*, 2001]. Thus, studying the climates of the Archean Earth is of prime interest to understand the environment in which life emerged and evolved.

[3] According to the standard model of stellar evolution, the Sun was 20 to 25% weaker during the Archean [*Gough*, 1981]. With such a weaker Sun, the Earth with the present-day atmospheric composition would fall into a full glaciation, hardly reconcilable with the evidence of liquid water and life during the whole Archean [*Sagan and Mullen*, 1972; *Feulner*, 2012]. This has been named the "faint young Sun problem" or the "faint young Sun paradox."

[4] While the Earth was unfrozen during most of the Archean, there is geological evidence for glaciations at the end of the Archean (the Huronian glaciations), between 2.45 and 2.22 Ga [*Evans et al.*, 1997]. These have been linked to the rise of oxygen in the atmosphere [*Kasting and Howard*, 2006; *Kasting and Ono*, 2006] and the destruction of atmospheric methane. There was also a possible glaciation at 2.9 Ga [*Young et al.*, 1998] but it would have been regional, not global, and its origin remains unknown [*Kasting and Ono*, 2006]. The Archean Earth therefore seems to have experienced very few glaciations, implying that there were temperate or hot climates during most of the Archean. However, the Archean rock record is extremely sparse and the latitudes of these geological data are unknown. Sea ice and continental ices could have existed at high latitudes, and other glaciations may have occurred.

[5] Paleotemperatures were estimated from the isotopic composition of marine cherts [*Knauth and Lowe*, 2003;

[1]Laboratoire de Météorologie Dynamique, Université Pierre et Marie Curie, Paris, France.
[2]Department of the Geophysical Sciences, University of Chicago, Chicago, Illinois, USA.

Corresponding author: B. Charnay, Laboratoire de Météorologie Dynamique, Université Pierre et Marie Curie, 4 place Jussieu, FR-75252 Paris CEDEX 05, France. (bclmd@lmd.jussieu.fr)

2169-897X/13/10.1002/jgrd.50808

Robert and Chaussidon, 2006] and indicate hot oceans (between 60°C and 80°C) during the Archean. This makes the faint young Sun problem even more challenging. The validity of these measurements has been questioned, however, because of the possible variation of the isotopic composition of oceans during the time [*Kasting and Howard*, 2006; *Kasting et al.*, 2006; *Jaffrés et al.*, 2007] and because of the impact of hot hydrothermal circulation on chert formation [*van den Boorn et al.*, 2007]. The most recent analyses obtained an upper limit at 40°C [*Hren et al.*, 2009; *Blake et al.*, 2010].

[6] Estimating the temperature of the oceans is also controversial as far as biological evidence is concerned. Genetic evolution models suggest that the ancestors of bacteria, eukaryota, and archaea were thermophylic during the Archean [*Gaucher et al.*, 2008; *Bousseau et al.*, 2008] consistent with the oceans at 60°C to 80°C. The environment of the last universal common ancestor has been estimated to be more temperate (around 20°C), suggesting an adaptation to high temperatures [*Bousseau et al.*, 2008] possibly in response either to a change in the climate of the early Earth, or to the strong impacts during the LHB. Yet these trends do not necessarily correspond to the climate of the Archean Earth, but maybe just reflect the environment where life was thriving. To avoid glaciation and allow such temperate or hot climates, the early Earth must have experienced warming processes.

1.2. Solutions to the Faint Young Sun Problem

[7] A different atmospheric composition with a larger amount of greenhouse gases was first proposed as the key to get a habitable Earth under a fainter Sun. The first studies examined ammonia (NH_3) [*Sagan and Mullen*, 1972], a strong greenhouse gas. However, ammonia would have had a short lifetime (less than 40 years) due to photolysis in the high atmosphere. It would therefore not have been present in sufficient amounts unless there was a large, permanent surface source [*Kuhn and Atreya*, 1979]. Yet such a permanent source would have produced so much N_2 (compared to present inventory) by photolysis of ammonia that it could not happen.

[8] Current thinking is that the early Earth had a CO_2- and CH_4-rich atmosphere. The amount of CO_2 in the atmosphere is controlled by the carbonate-silicate cycle [*Walker et al.*, 1981], which acts as a thermostat on the climate, preserving Earth from a full glaciation by injecting CO_2 from volcanoes in the atmosphere. CO_2 may have reached large amounts during the early Earth, although the maximum is not well known (between 0.1 and 10 bars [*Walker*, 1985; *Sleep and Zahnle*, 2001]). According to 1-D models [*von Paris et al.*, 2008; *Pavlov et al.*, 2000], with a 20% weaker Sun, $\sim$0.03 bar of CO_2 is required to raise the temperature above the frost point and $\sim$0.2 bar to get present-day temperatures. However, geochemical data from paleosols constrain the maximum partial pressure of CO_2 to around 0.02 bar for the end of the Archean [*Rye et al.*, 1995; *Sheldon*, 2006; *Driese et al.*, 2011; *Feulner*, 2012], 10 times lower than what is required to get a temperate climate. A stronger constraint of 0.9 mbar of CO_2 has been obtained [*Rosing et al.*, 2010] based on the coexistence of siderite and magnetite in Archean-banded iron formations. However, this contradicts other measurements [*Hessler et al.*, 2004; *Sheldon*, 2006; *Driese et al.*, 2011] and is currently debated [*Reinhard and Planavsky*, 2011].

[9] Methane has been suggested as an important complement to CO_2 to warm the early Earth [*Kiehl and Dickinson*, 1987]. It can absorb thermal radiation at 7–8 μm, thus at the edge of the atmospheric window (8–12 μm), where CO_2 cannot. It can therefore produce an efficient warming. In an anoxic atmosphere, the lifetime of methane is 1000 times higher than today [*Zahnle*, 1986; *Kasting and Howard*, 2006]. During the Archean, methane would have been released by methanogenic bacteria through the reaction:

$$CO_2 + 4H_2 \Rightarrow CH_4 + 2H_2O \quad (1)$$

where H_2 comes from hydrothermal sources and volcanoes, or from the primitive atmosphere [*Tian et al.*, 2005].

[10] With the present-day biological flux, the Archean atmosphere would contain around 3 mbar of methane [*Kasting and Howard*, 2006]. Based on the biological flux and the escape rate of hydrogen, the amount of methane is estimated to be on the order of 1 mbar during the Archean, with a plausible range between 0.1 mbar and 35 mbar [*Kharecha et al.*, 2005]. However, the time when methanogens appeared and diversified is still highly uncertain. Attempts to determine this time have been made using genomic evolution models [*Battistuzzi et al*., 2004; *House et al*., 2003] but the resulting times range from the beginning to the end of the Archean.

[11] Before methanogens appeared or when they were confined to hydrothermal vents, methane was present in the atmosphere but in lower amounts. *Tian et al.* [2011] estimate around $0.5–5 \times 10^{-3}$ mbar of methane for the prebiotic atmosphere, based on emanations from the Lost City hydrothermal vent field studied by *Kelley et al.* [2005].

[12] If the mixing ratio of methane is large, an organic haze forms. This is expected to happen when the CH_4/CO_2 ratio becomes higher than 0.1–0.3 according to photochemical models and experimental data [*Zerkle et al.*, 2012; *Trainer et al.*, 2006]. In addition to limiting the amount of methane, the formation of haze could produce an anti-greenhouse effect [*McKay et al.*, 1991; *Haqq-Misra et al.*, 2008; *Kasting and Ono*, 2006], and hence cool the Earth. The impact of this anti-greenhouse effect on surface temperature is unknown, mostly because the fractal nature of haze particles is unconstrained. Fractal particles produce a limited anti-greenhouse effect, compared to spherical particles. Moreover, they act as a UV shield, like the ozone layer, protecting both life and photolytically unstable reduced gases [*Wolf and Toon*, 2010]. Under this shielding, ammonia may have been maintained in sufficient amount to solve the faint young Sun problem.

[13] In any event, measurements of carbon isotopes appear consistent with a methane-rich atmosphere at the end of the Archean with possible episodic formation of haze [*Zerkle et al.*, 2012]. According to the 1-D model of *Haqq-Misra et al.* [2008], which includes haze formation, 1 mbar of methane in an atmosphere containing 20 mbar of CO_2 allows to reach present-day temperatures at the end of the Archean. However, an ice-free Earth cannot be maintained with only a CO_2-CH_4 greenhouse warming consistent with the geological constraints for CO_2.

[14] Given the difficulties in reconciling the warm temperatures estimated for the Archean with geological constraints for CO_2, other mechanisms of warming than greenhouse gases have been explored. Clouds both warm the surface by absorbing and reemitting infrared radiation and cool it by reflecting sunlight in the visible. Through these mechanisms, lower clouds tend to globally cool the Earth, while higher clouds tend to warm it. A negative feedback, increasing the amount of cirrus (higher clouds), was considered to keep the climate clement, the "Iris hypothesis" [*Lindzen et al*., 2001; *Rondanelli and Lindzen*, 2010], but remains controversial [*Lin et al.*, 2002; *Goldblatt and Zahnle*, 2011b]. A more plausible hypothesis is that lower clouds were optically thinner during the Archean, owing to the lack of cloud condensation nuclei from biological sources, which yields a decrease of the planetary albedo, and hence a warming ($\sim +10°C$) [*Rosing et al.*, 2010].

[15] The planetary albedo has been suggested to be lower in the Archean because of the reduced surface of emerged continents [*Rosing et al.*, 2010]. It has also been proposed that the pressure was higher in the past, because the equivalent of around 2 bars of nitrogen is present in the Earth's mantle [*Goldblatt et al.*, 2009]. That nitrogen, initially in the atmosphere, should have been incorporated by subduction (probably by biological fixation). Therefore, it is plausible that the partial pressure of nitrogen reached 2 to 3 bars during the Archean. According to 1-D modeling, doubling the amount of present-day atmospheric nitrogen would cause a warming of 4–5°C [*Goldblatt et al.*, 2009]. Besides, hydrogen could have been abundant in the early Earth's atmosphere. The lack of O_2 would have led to a cooler exosphere limiting the hydrogen escape. Thus, the balance between hydrogen escape and volcanic outgassing could have maintained a hydrogen mixing ratio of more than 30% [*Tian et al.*, 2005].

[16] The combination of a hydrogen-rich atmosphere with a higher atmospheric pressure (2 to 3 bars) would produce an important greenhouse effect by collision absorption of H_2-N_2, sufficient to get present-day temperatures with a limited amount of CO_2 [*Wordsworth and Pierrehumbert*, 2013]. These mechanisms remain to be further explored. They might not be sufficient to solve the faint young Sun problem alone, although they probably played a role in maintaining a clement climate, complementing the greenhouse effect by CO_2 and methane.

1.3. Previous Modeling Studies

[17] Given the paucity of available data for the early Earth, climate modeling is particularly useful to explore and understand the evolution of the atmosphere and the climate. One-dimensional radiative-convective models allow different hypotheses to solve the faint young Sun problem to be tested [*Owen et al.*, 1979; *Kasting et al.*, 1984; *Kiehl and Dickinson*, 1987; *Kasting and Ackerman*, 1986; *Haqq-Misra et al.*, 2008; *von Paris et al.*, 2008; *Domagal-Goldman et al.*, 2008; *Goldblatt et al.*, 2009; *Rosing et al.*, 2010]. However, such models calculate the mean surface temperature below a single atmospheric column with averaged solar flux. Clouds are often omitted, or widely fixed (altitude, optical depth, and covering). Furthermore, the transport of energy by the atmosphere and the ocean is not taken into account in 1-D modeling. The continental and oceanic ice formation is not accounted for either. Thus, 1-D radiative-convective models fail to capture both cloud and ice-albedo feedbacks and transport processes, which are fundamental to determine the climate sensitivity under different conditions. Moreover, the lack of clouds in 1-D radiative-convective models can lead to overestimates of the radiative forcing of greenhouse gases [*Goldblatt and Zahnle*, 2011b].

[18] The most accurate way to simulate the climate is to use 3-D global climate models (GCMs), including more of the fundamental processes which control climate sensitivity (e.g., clouds, oceanic transport, continental and oceanic sea ice). Studies of the Archean Earth using GCMs are rare. However, preliminary GCM studies showed that the absence of an ozone layer, continent, and a faster rotation rate could modify cloud coverage and hence the surface temperature [*Jenkins*, 1993; *Jenkins et al.*, 1993; *Jenkins*, 1995, 1999]. Using a 3-D oceanic model coupled to a parameterized atmospheric model, *Kienert et al.* [2012] explored the key role of the ice-albedo feedback and found that 0.4 bar of CO_2 is required to avoid full glaciation. This illustrates the key role of ice-albedo feedback.

[19] We describe below the application of a new generic GCM recently developed by our team to Archean climates. The versatility of this model allowed us to explore the climates of the Archean Earth under many conditions discussed in the literature (such as greenhouse gases, atmospheric pressure, and rotation rate). Our goal is to test different warming processes suggested by 1-D models to better constrain the Archean climate and address key questions left unresolved by 1-D models.

2. Description of the Model

2.1. Generalities

[20] We use a new generic version of the Laboratoire de Météorologie Dynamique (LMD) global climate model recently developed to simulate a complete range of planetary atmospheres. This model has been used to study early climates in the solar system [*Forget et al.*, 2012; *Wordsworth et al.*, 2012] as well as climates on extrasolar planets [*Wordsworth et al.*, 2011; *Leconte et al.*, 2013]. The model is derived from the LMDz Earth GCM [*Hourdin et al.*, 2006], which solves the primitive equations of meteorology using a finite difference dynamical core on an Arakawa C grid. This dynamical core has been tested in a variety of atmospheres such as the present Earth [*Hourdin et al.*, 2006], Mars [*Forget et al*., 1999], Venus [*Lebonnois et al*., 2010], and Titan [*Lebonnois et al.*, 2012; *Charnay and Lebonnois*, 2012].

[21] In this paper, simulations were performed with a horizontal resolution of 64×48 (corresponding to resolutions of 3.75° latitude by 5.625° longitude). In the vertical, the model uses hybrid coordinates, that is, a terrain-following σ coordinate system (σ is pressure divided by surface pressure) in the lower atmosphere, and pressure levels in the upper atmosphere. In this work, we used 20 layers, with the lowest midlayer level at 4 m and the top level at 3 hPa (>50 km). Nonlinear interactions between explicitly resolved scales and subgrid-scale processes are parameterized by applying a scale-selective horizontal dissipation operator based on an n time iterated Laplacian Δ^n. This can be written as $\partial q/\partial t = ([-1]^n/\tau_{\mathrm{diss}})(\delta x)^{2n}\Delta^n q$ where δx is the

smallest horizontal distance represented in the model and τ_{diss} is the dissipation timescale for a structure of scale δx. Subgrid-scale dynamical processes (e.g., turbulent mixing and convection) are parameterized as in *Forget et al.* [1999]. In practice, the boundary layer dynamics are accounted for by *Mellor and Yamada* [1982] unstationary 2.5-level closure scheme, plus a convective adjustment which rapidly mixes the atmosphere in the case of dry unstable temperature profiles. Turbulence and convection mix energy (potential temperature), momentum (wind), and water vapor. A standard roughness coefficient of $z_0 = 10^{-2}$ m is used for both rocky and ocean surfaces for simplicity. The evolution of surface temperature is governed by the balance between radiative fluxes (direct solar insolation and thermal radiation from the atmosphere and the surface), turbulent and latent heat fluxes, and thermal conduction in the soil. The parameterization of this last process is based on an 18-layer soil model solving the heat diffusion equation using finite differences. The depth of the layers was chosen to capture diurnal thermal waves as well as the deeper annual thermal wave. A vertically homogeneous soil is assumed. The thermal inertia for ground is set to 2000 J $s^{-1/2}$ m^{-2} K^{-1} everywhere.

[22] In equilibrium, the globally averaged difference between outgoing longwave radiation and absorbed solar radiation was found to be lower than 2 W/m^2. Simulations were typically run for 40 years for temperate climates. For cold climates, the equilibrium is reached after a longer time. We ran simulations for 80 years to be sure not to miss a full glaciation.

2.2. Radiative Transfer

[23] Our radiative scheme is based on the correlated k model as in *Wordsworth et al.* [2011], with absorption for H_2O, CO_2, and CH_4 calculated directly from high-resolution spectra obtained by a line-by-line model that uses the HITRAN 2008 database [*Rothman et al.*, 2009]. At a given pressure and temperature, correlated k coefficients in the GCM are interpolated from a matrix of coefficients stored in a 7 × 9 temperature and log-pressure grid: T = 100, 150, 200, 250, 300, 350, 400 K, $p = 10^{-1}, 10^{0}, 10^{1}, \ldots, 10^{7}$ Pa. We used 36 spectral bands in the thermal infrared and 38 at solar wavelengths. Sixteen points were used for the g-space integration, where g is the cumulated distribution function of the absorption data for each band.

[24] The radiative transfer code used the two stream scheme from *Toon et al.* [1989]. Rayleigh scattering by N_2 and CO_2 molecules was included using the method described in *Hansen and Travis* [1974]. The water vapor continuum from *Clough et al.* [1992] is included. This is important essentially for hot climates. An improved collision-induced absorption for CO_2 is used [*Wordsworth et al.*, 2010]. This effect is important in the case of a high CO_2 partial pressure but remains small for the simulation presented in this paper. The sub-Lorentzian profiles of *Perrin and Hartmann* [1989] are used for the CO_2 far line absorption.

[25] The model predicts the cloud cover at each grid mesh. For each column, a global cloud cover is fixed equal to the cover of the optically thicker cloud. We therefore take as a reference the thickest cloud rather than the widest cloud. This avoids the bias induced by thin stratospheric clouds, which can have a cover up to 100% for an atmosphere without ozone. Then, we assume that each individual cloud cover is equal to this global cover with a maximum overlap. Radiative transfer is therefore computed twice: in a clear sky column, and in a cloudy sky column whose area is equal to the global cloud cover.

2.3. Water Cycle

2.3.1. Cloud Formation

[26] Cloud formation is computed through a moist convective scheme [*Manabe and Wetherald*, 1967] and a large-scale condensation scheme [*Le Treut and Li*, 1991]. We have chosen the Manabe and Wetherald scheme rather than the Betts-Miller scheme because it is more robust for a wide range of pressure, at the cost of giving enhanced precipitation at the equator [*Frierson*, 2007]. The large-scale condensation scheme predicts a cloud cover for every cell in the atmosphere. The latent heat between icy and liquid phase for cloud is not taken into account. Supercooling is taken into account, allowing liquid droplet down to –18°C. The percentage of liquid water in the condensed phase is given by

$$R_{\mathrm{liq/condensed}} = \frac{T - (273.15 - 18)}{18} \tag{2}$$

with T the temperature in K. For temperature higher (lower) than 273.15 K (255.15 K), clouds are only composed of liquid (ice) droplets.

[27] The radius of cloud droplet is fixed (12 μm for liquid droplet and 35 μm for icy droplet for modern Earth).

2.3.2. Precipitation

[28] Water precipitation is divided into rainfall and snowfall. We consider for both cases that precipitation is instantaneous (i.e., it goes directly to the surface) but can evaporate while falling through subsaturated layers.

[29] Rainfall is parameterized using the scheme from *Boucher et al.* [1995]. Conversion of cloud liquid droplets to raindrops occurs by coalescence with other droplets. The variations of cloud liquid water mixing ratio are given by

$$\frac{\mathrm{d}q_l}{\mathrm{d}t} = -c\alpha\rho_{\mathrm{air}}q_l^2 r_l \tag{3}$$

where c is a coefficient smaller than unity (we take $c = 0.6$ to match the observations on present-day Earth), $\alpha = 1.3 \times 10^5$ m^2 kg^{-1} s^{-1}, ρ_{air} is the air volume mass and r_l is the cloud droplet radius.

[30] Snowfall is calculated using the falling velocity v_i of icy particles. The variation of the cloud ice water mixing ratio is given by

$$\frac{\mathrm{d}q_i}{\mathrm{d}t} = -\frac{q}{\Delta z}v_i \tag{4}$$

where Δz is the depth of the layer in the model. Thus, we assume that what exits in a layer falls to the ground instantaneously. The falling velocity v_i is taken equal to the terminal velocity for ice crystals [*Langleben*, 1954; *Sekhon and Srivastava*, 1970]:

$$v_i = 10.6 \times r_i^{0.31} \tag{5}$$

with v_i in m/s and r_i, the ice crystal radius, in meters. We chose this parameterization fine tuned for the terrestrial case rather than a more general Stokes sedimentation scheme because the particular shape of snowflakes is better accounted for. This parameterization is only valid for the Earth with a background mean molar mass pretty similar to the present day, which is the case in our simulations.

[31] For evaporation of rain and snow during the fall in the atmosphere, we use the following formula [*Gregory*, 1995]:

$$e = 2 \times 10^{-5}(1 - RH)\sqrt{P} \tag{6}$$

where e is the evaporation rate (in kg/m^3/s), RH is the relative humidity, and P the precipitation flux (in kg/m^2/s).

2.3.3. Hydrology and Evaporation

[32] The ground is modeled as a simple bucket model with a maximum water capacity of 150 kg/m^2. When the water quantity exceeds this limit, the surplus is regarded as runoff and added to the ocean. Snow/ice over ground is treated the same way, though with maximal limit of 3000 kg/m^2. The melting (formation) of snow/ice is computed with latent heat exchange when the surface temperature is lower (higher) than 273.15 K.

[33] The ground albedo A rises with the quantity of snow/ice up to a maximum value ($A_{\max}$=0.55) as

$$A = A_{\text{initial}} + (A_{\max} - A_{\text{initial}}) \times q_{\text{ice}}/q_* \tag{7}$$

with q_{ice} the amount of snow/ice on the surface and $q_* = 33$ kg/m^2 (corresponding to a uniform layer of approximately 3.5 cm thickness [*Le Treut and Li*, 1991]).

[34] Evaporation E is computed within the boundary layer scheme, using a bulk aerodynamic formula multiplied by a dryness coefficient β:

$$E = \beta \rho_{\text{air}} C_d V (a_s - a_a) \tag{8}$$

$$\beta = \min\left(1, 2\frac{q}{150}\right) \tag{9}$$

$$C_d = \frac{\kappa}{\ln(1 + z_1/z_0)} \tag{10}$$

with V the wind speed at the first level, ρ the air density, a_s and a_a the absolute humidity at the surface and at the first level, q the mass of water (liquid + solid) at the surface (in kg/m2), κ the constant of von Karman (=0.4), z_0 the roughness, and z_1 the altitude of the first level. Over the ocean, $\beta = 1$.

2.4. Oceanic Transport and Sea Ice

[35] The ocean and the sea ice are important components of the Earth's climate. A full ocean general circulation model would, however, be too expensive for our study, because of the long integrations required for complete adjustment to the many different conditions imposed (changing luminosity, continental extent, atmospheric composition, and so on). Moreover such precision is not required given the large number of unknown parameters. We therefore use a simplified ocean model with fast adjustment, concentrating on a representation of the essential components for the global climate: the oceanic heat transport and the sea ice extent.

[36] We use the ocean model from *Codron* [2012], which uses the same horizontal grid as the GCM. This model is composed of two layers. The first layer (50 m depth) represents the surface mixed layer, where the exchanges with the atmosphere take place. The second layer (150 m depth) represents the deep ocean. The transport of heat by the ocean circulation is given by two components. First, the impact of subgrid-scale eddies is represented by horizontal diffusion, with a uniform diffusivity in both layers. Then, the mean wind-driven circulation is computed by calculating the Ekman mass fluxes in the surface layer from the surface wind stress and taking an opposite return flow at depth. These mass fluxes are then used to advect the ocean temperature horizontally. In the case of divergent horizontal mass fluxes, the upwelling or downwelling mass flux is obtained by continuity. Other components of the ocean circulation—density-driven circulations and horizontal gyres—are not present in the model. Although they can play an important role regionally on the present Earth, they are weaker on global average, and gyres would be absent in the case of a global ocean. This simplified model reproduces the global meridional oceanic heat transport quite closely compared to a full GCM, both for actual Earth and for a simulated global ocean case [*Marshall et al.*, 2007].

[37] The oceanic model also computes the formation of oceanic ice. Sea ice forms when the ocean temperature falls below –1.8°C and melts when its temperature rises above freezing. The changes in ice extent and thickness are computed based on energy conservation, keeping the ocean temperature at –1.8°C as long as ice is present. A layer of snow can be present above the ice. The surface albedo is then that of snow, or for bare ice:

$$A = A_{\text{ice}}^{\max} - (A_{\text{ice}}^{\max} - A_{\text{ice}}^{\min}) \exp(-h_{\text{ice}}/h_{\text{ice}}^0) \tag{11}$$

with A the albedo, $A_{\text{ice}}^{\max} = 0.65$ the maximal albedo, $A_{\text{ice}}^{\min} = 0.2$ the minimal albedo, h_{ice} the ice thickness (in m) and $h_{\text{ice}}^0 = 0.5$ m. The albedo over the ice-free ocean is taken to be equal to 0.07. The value for the maximal sea ice albedo we used (i.e., 0.65) is classical for GCMs. It is a pretty high value for studies of snowball Earth [*Abbot et al.*, 2011], making our results concerning cold climates pretty robust.

[38] The transport of sea ice is not taken into account. This has a small impact for the present-day conditions, but it may be more important for different conditions (e.g., a colder climate with more sea ice) [*Lewis et al.*, 2003].

3. Model Verification on Modern Earth

3.1. Simulation of the Modern Earth

[39] Before starting to investigate Earth's early climates, it is important to check the model's performance by simulating the present Earth. For verification, we compare the simulations we get with National Centers for Environmental Prediction/National Center for Atmospheric Research (NCEP/NCAR) reanalysis (www.esrl.noaa.gov/psd/data).

[40] We use 360 × 180 resolution maps for topography and ground albedo which are interpolated on the GCM grid. The average surface pressure is 1013 mbar, which is a little higher than the reality because of the topography. Yet the impact of this small change is negligible.

[41] The atmosphere is composed of N_2 with CO_2 and CH_4 at present-day levels (0.375 mbar of CO_2 and 1.75×10^{-3} mbar of CH_4). We do not include O_2 and ozone for simplicity in the radiative transfer calculation. The absence of O_2 has no strong impact (changes in Rayleigh scattering and heat capacity are small). The absence of ozone implies the absence of a temperature inversion in the stratosphere. The consequences of this assumption are discussed briefly in the next section. As far as astronomical parameters are concerned, we use the present-day obliquity (23.44°), eccentricity (0.0167), and solar constant (1366 W/m^2).

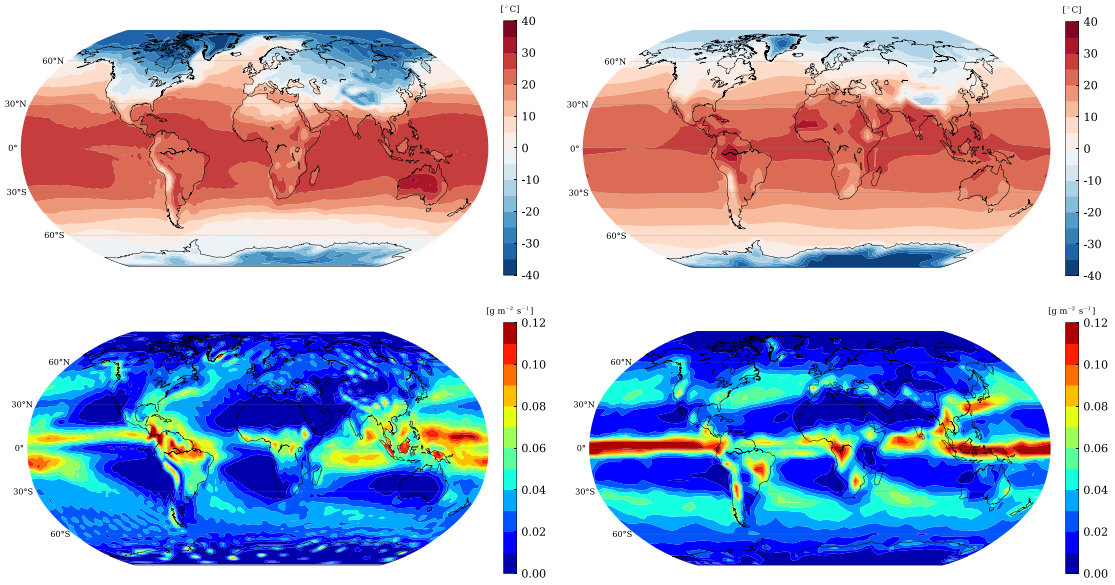

Figure 1. Annually averaged (top row) surface temperature and (bottom row) precipitation on the Earth from (left column) NCEP/NCAR reanalysis and from (right column) our GCM.

[42] In our Earth-like simulation, we find an average surface temperature of 14.9°C (compared to 15.0°C in NCEP reanalyses) and an average planetary albedo of 0.36 (compared to 0.33). This higher albedo in our model is due to a higher amount of clouds produced at the Intertropical Convergence Zone (ITCZ) and the absence of ozone, which decreases solar atmospheric absorption and increases the higher clouds (see next paragraph). Since higher clouds are enhanced, their greenhouse effect increases and compensates the albedo cooling. Thus, the surface temperature is not much affected. Figure 1 (top row) shows the annual average surface temperature simulated by our model and from the NCEP/NCAR reanalysis. The tropical seas are a little colder (0.8°C colder at the equator and 1.9°C over all the tropics) in our model and the northern polar regions are warmer (15°C warmer). Therefore, our GCM produces higher temperatures at high latitudes, maybe due to a too strong meridional transport or a cloud effect. In the northern polar region, this is strongly amplified by sea ice which disappears in summer. If the sea ice was still present in summer, the temperatures would be far lower as in the Southern Hemisphere. Our model also produces a colder western Pacific warm pool. The difference of sea surface temperature is around 2–3°C between western and eastern Pacific at the equator, thus less than the $\sim$ 5°C observed.

[43] Figure 1 (bottom row) shows the annual average precipitation simulated by our model and from the NCEP/NCAR reanalysis. Our model produces too much precipitation over the ITCZ in Pacific Ocean. This is certainly due to our moist convection scheme, as explained in *Frierson* [2007]. The precipitation over the tropics and midlatitudes is accurate with rain over Amazonia and very little rain over the Saharan and Arabian deserts.

[44] To conclude, the temperatures and precipitations are globally close to the NCEP/NCAR reanalysis. Even if our model does not reproduce perfectly the latitudinal gradient and regional temperatures, it simulates the terrestrial climate with sufficient accuracy for the goals of this study (i.e., to simulate global climates, 3-D effects and good trends for paleoclimates). Indeed, having prognostic equations for the cloud properties and distribution, the predictive ability of 3-D models is enhanced when compared to 1-D models, even when looking only at the global scale.

3.2. Effect of the Ozone and the Oceanic Transport

[45] The present ozone layer absorbs around 7 W/m^2 of the solar flux at UV wavelengths, producing the stratospheric thermal inversion. This absorption tends to cool the surface but it is compensated by the greenhouse effect of the ozone. For radiative-convective models, the presence of ozone yields a warming of the surface [*Francois and Gerard*, 1988]. The presence of ozone impacts the tropospheric dynamics [*Kiehl and Boville*, 1988] and also leads to a warmer higher troposphere, which could result in a decrease of the amount of cirrus clouds, reducing their greenhouse effect [*Jenkins*, 1995]. If ozone is added, both effects (the increase of solar atmospheric absorption and the decrease of amount of higher clouds) should decrease the planetary albedo without changing surface temperature very

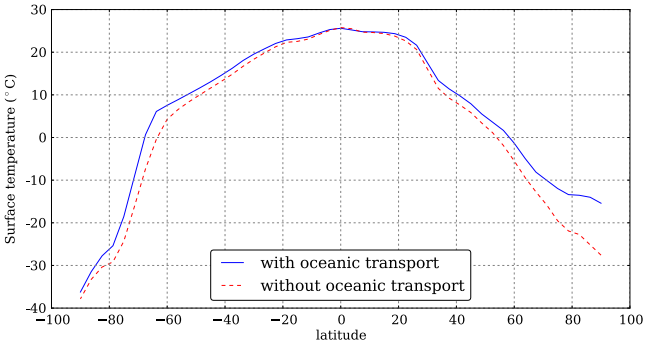

Figure 2. Zonally averaged surface temperature on the modern Earth with (blue) and without (red) oceanic transport.

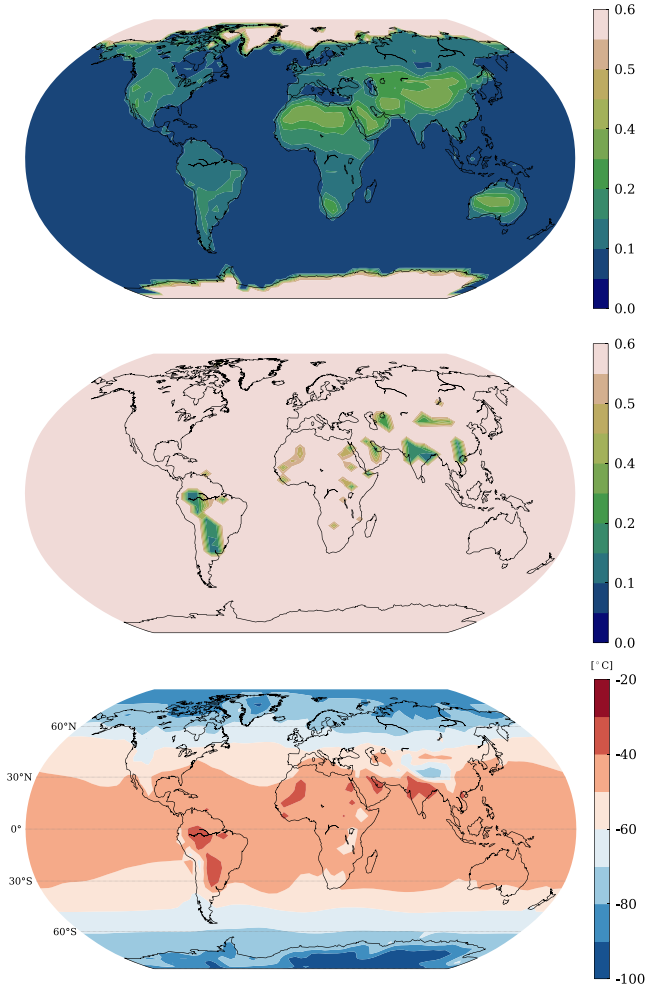

Figure 3. Surface albedo (top) at the beginning and (middle) after 23 years of simulation of the present-day Earth under a 20% weaker Sun and leading to a full snowball Earth. (bottom) Mean surface temperature after 23 years of simulation.

much. This should partially explain the bias for the albedo in our model.

[46] Other 3-D simulations with and without ozone will be required to estimate precisely the impact of ozone.

[47] The heat transport by the ocean can impact the mean global surface temperature. Under present-day conditions, the oceanic transport limits the spreading of sea ice and thus the ice-albedo feedback. This leads to a global warming of the Earth. Figure 2 shows the effect of the oceanic transport for Earth. Without oceanic transport, sea ice cover rises, yielding a decrease of $\sim 2°C$ for the mean surface temperature and a decrease of 12°C at the northern pole. Thus, the oceanic transport has a moderate impact in our model.

4. Simulation of the Archean Earth

[48] In this section, we apply our model to the Archean Earth under a fainter Sun. We explore the effects of land distribution and greenhouse gases over the whole duration of the Archean.

4.1. Testing the Faint Young Sun Problem

[49] First, we ran the model with the present-day continents and atmosphere under a 20% weaker Sun (corresponding to the Sun 3 Ga) to illustrate the faint young Sun problem. Figure 3 shows the resulting glaciation with the spreading of sea ice from the polar region to the equator. A full "snowball Earth" is produced after only 23 years. The equilibrium mean surface temperature is –54°C. Moreover, if we reset the solar insolation to its modern value, the Earth does not exit from the snowball state and remains entirely frozen.

4.2. Choice of Land Distribution, Greenhouse Gases and Solar Irradiance

[50] The fraction of the Earth covered by land was different during the Archean than at the present time. The continental crust volume was lower and has increased during the Archean [*Belousova et al.*, 2010; *Dhuime et al.*, 2012]. Thermal modeling and hypsometry indicate that most continents were flooded throughout the Archean [*Flament et al.*, 2008]. In addition, the ocean volume may have been up to 25% greater than today [*Pope et al.*, 2012]. Thus, it is realistic to believe that the fraction of emerged land was low. Lands could have emerged essentially at the end of the Archean [*Flament et al.*, 2008]. This has been suggested as the key element triggering the Great Oxidation Event, associated with the change in the oxidation state of volcanic gases transiting from submarine to aerial volcanism [*Kump and Barley*, 2008; *Gaillard et al.*, 2011]. In this study, we consider three periods of the Archean for which we run simulations: the beginning at 3.8 Ga, the middle at 3 Ga, and the end at 2.5 Ga. For simplicity, we make the hypothesis that land appears after 3 Ga and that there was little land before. Thus, we run the model with no land for 3.8 and 3 Ga and with a flat equatorial supercontinent covering 20% of the Earth at 2.5 Ga. An equatorial supercontinent is the ideal case to keep ice-free land. If ice-free land cannot be maintained with a supercontinent at the equator, then it would be the same at any location. The boundaries of the supercontinent are $\pm 38°$ in latitude and $\pm 56°$ in longitude, and the altitude is zero for simplicity. The albedo of Archean land is unknown. We have chosen an albedo of 0.3, which is relatively large even for a surface without vegetation (for comparison, the Moon's albedo is under 0.15). This maximizes the cooling effect of land and gives us robust conclusions concerning the impact of land distribution. We discuss this in the next section.

[51] Concerning the atmosphere, most of the simulations are performed with one of the following three atmospheric compositions:

[52] 1. Composition A: a low level of CO_2 (0.9 mbar of CO_2 and CH_4) corresponding to the composition from *Rosing et al.* [2010].

[53] 2. Composition B: an intermediate level of CO_2 (10 mbar of CO_2 and 2 mbar of CH_4) corresponding approximately to the maximal amount of CO_2 and CH_4 consistent with the geological constraints at the end of the Archean (see section 1).

[54] 3. Composition C: a high level of CO_2 (0.1 bar of CO_2 and 2 mbar of CH_4).

[55] Compositions A and B could lead to the formation of organic hazes, yet we ignore their impact. The mean surface

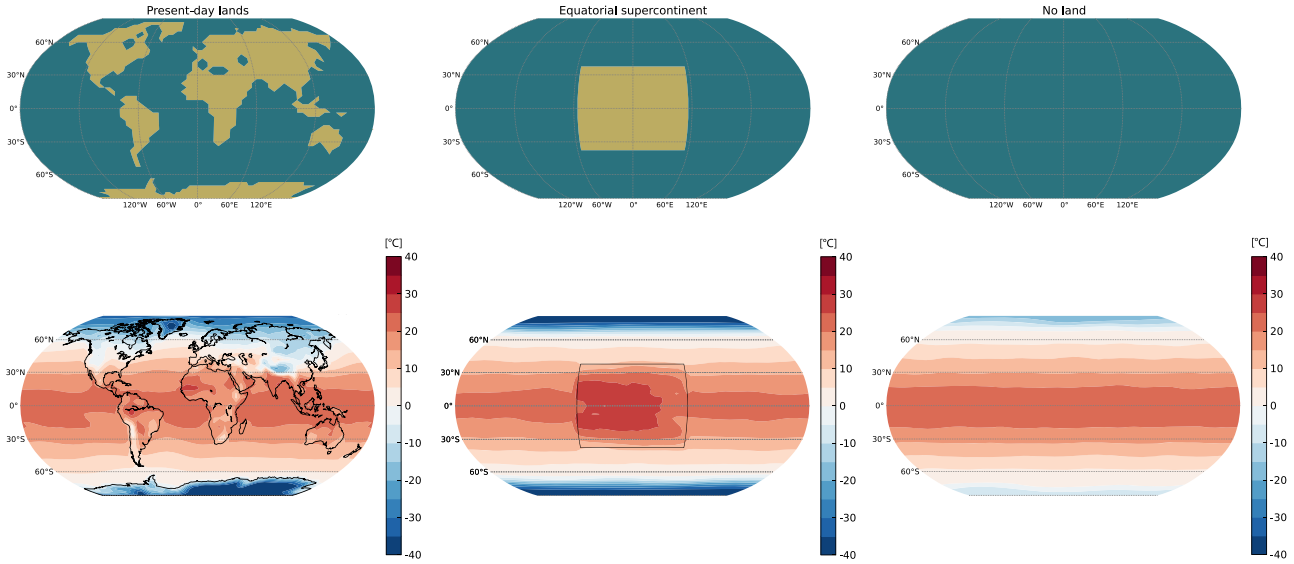

Figure 4. (top row) Continents and (bottom row) mean surface temperature for (left column) present-day lands, (middle column) an equatorial supercontinent, and (right column) no land at 2.5 Ga (atmospheric composition: 10 mbar of CO_2 and 2 mbar of CH_4).

pressure is taken equal to 1 bar for simplicity in all cases, completing the rest of the atmosphere with N_2. Hence, we use a partial pressure of N_2 higher than today (0.8 bar). This may have been the case, yet the impact of 0.2 additional bar of N_2 remains limited (see section 5.2.).

[56] Concerning the astronomical parameters, we used the present-day obliquity but no eccentricity for the orbit. The solar luminosity L of the Archean Sun has been fixed in our simulation by the formula of *Gough* [1981]:

$$L(t) = \left[1 + \frac{2}{5}\left(1 - \frac{t}{t_\odot}\right)\right]^{-1} L_\odot \qquad (12)$$

where t is the time before today, $t_\odot$ = 4.57 Gyr is the age of the solar system, and $L_\odot = 3.85 \times 10^{26}$ W is the modern solar luminosity. If we use a solar constant of 1366 W/m^2 for the modern Sun, we get a solar constant for the Archean Sun of 1120.8, 1081.9, and 1025.1 W/m^2 at 2.5, 3, and 3.8 Ga. respectively.

4.3. Effect of Lands

[57] According to 1-D models, in the absence of organic haze, composition B is sufficient to get a temperate climate at 2.8 Ga [*Haqq-Misra et al.*, 2008]. Therefore, we chose this composition to assess the influence of emerged land at the end of the Archean at 2.5 Ga. Figure 4 shows the annually averaged surface temperatures obtained with either present-day land, the equatorial supercontinent, or no land. We get a mean surface temperature of 10.5°C with present-day land, 11.6°C with the equatorial supercontinent, and 13.8°C with no land (see Table 1). In all cases, we get colder climates than today. For the present-day land, we get more continental ice at high latitudes. Although no traces of glaciation have been observed for most of the Archean, that could be acceptable given the few data available and the impossibility of determining their latitudes. In the simulation with the supercontinent, we get a desert climate with very little precipitation and warm temperatures on the continent. This case would be consistent with the absence of glaciation for most of the Archean [*Kasting and Ono*, 2006]. For the Earth with no land, we get a warmer ocean than in the other cases and less sea ice at the poles. We can conclude that land, regardless of its location, has a limited impact on the mean surface temperature. The removal of all land compared to present-day leads a to a global warming of 3.3°C (see Table 1). The mean tropical oceanic temperature is even less affected (a difference of less than 1.5°C). We found a planetary albedo of 0.34 with present-day land and 0.33 for the supercontinent and no land. The removal of land produces a radiative forcing of ∼10 W/m^2 for present-day land and only ∼2 W/m^2 for the supercontinent. Thus, the planetary albedo is approximately the same with the equatorial supercontinent than with no land, even assuming a high ground albedo of 0.3.

[58] Contrary to what was deduced from 1-D models [*Rosing et al.*, 2010], the presence of land, not covered with ice, does not necessarily increase the planetary albedo.

Table 1. Global Mean Values Obtained With the GCM for the Modern Earth and for the Archean Earth at 2.5 Ga With Present-Day Land, the Equatorial Supercontinent and No Land (Atmospheric Composition: 10 Mbar of CO_2 and 2 Mbar of CH_4)

Land Distribution	Mean Surface Temperature	Tropical Oceanic Temperature	Planetary Albedo	Precipitable Water	Condensed Water
Modern Earth (present Sun)	14.8°C	23.7°C	0.36	18.15 kg/m^2	0.16 kg/m^2
Present-day land	10.5°C	20.0°C	0.34	14 kg/m^2	0.135 kg/m^2
Equatorial supercontinent	11.6°C	19.4°C	0.33	13.2 kg/m^2	0.12 kg/m^2
No land	13.8°C	20.8°C	0.33	16 kg/m^2	0.15 kg/m^2

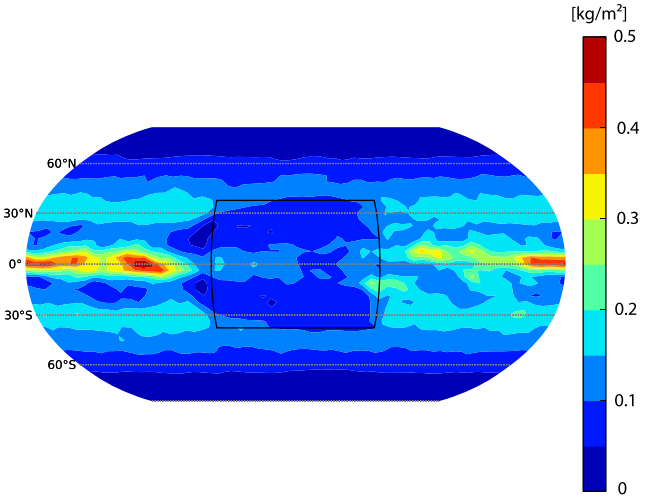

Figure 5. Column of condensed water (liquid and icy clouds) with an equatorial supercontinent at 2.5 Ga (atmospheric composition: 10 mbar of CO_2 and 2 mbar of CH_4).

There are generally less clouds over lands than over oceans. This is observed on the present-day Earth with less clouds in the Northern Hemisphere than in the Southern Hemisphere, and this is clear in our simulations in the case of the supercontinent. Figure 5 shows the lack of clouds over the supercontinent. This is caused by the lower evaporation over lands and the subsidence zones forming over them. Yet even with a similar planetary albedo, the absence of land leads to a higher mean surface temperature owing to the larger amount of water vapor in the atmosphere resulting from more evaporation (see Table 1). This larger amount of water vapor also enhanced transport of energy to the poles which become warmer (compare surface temperatures for the case with the supercontinent and the case with no land in Figure 4).

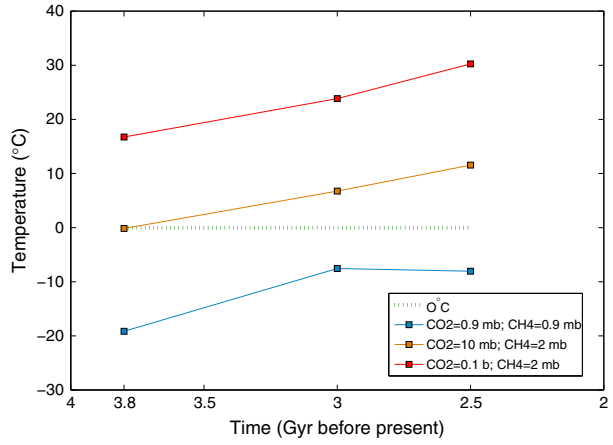

Figure 6. Mean surface temperature during the Archean with 0.9 mbar of CO_2 and CH_4 (blue line), 10 mbar of CO_2 and 2 mbar of CH_4 (orange line), and 0.1 bar of CO_2 and 2 mbar of CH_4 (red line). Dotted green line corresponds to the freezing point of water.

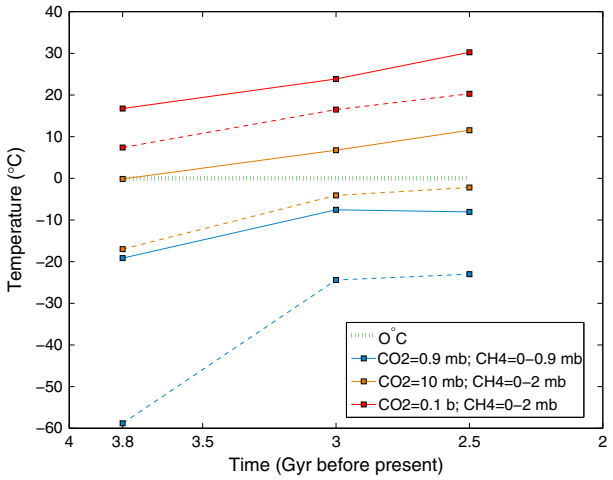

Figure 7. Same as Figure 6. Dashed lines correspond to atmospheric composition without methane.

4.4. Effect of Greenhouse Gases

[59] Figure 6 shows the mean surface temperature obtained with our model throughout the Archean with the three atmospheric compositions defined previously. The simulations have been run with the hypothesis for lands from section 4.3, no land at 3.8 and 3 Ga, and a supercontinent at 2.5 Ga. Composition B, which gives climates close to the present-day for the end of the Archean, is clearly not sufficient to get temperate climates at the beginning of the Archean (mean surface temperature around 0°C at 3.8 Ga). A stronger greenhouse effect is required. Composition C, with 0.1 bar of CO_2, allows for a temperate climate, even warmer than today, in the early Archean (mean surface temperature around 17°C at 3.8 Ga). Composition A yields mean surface temperature below the freezing point and will be studied in the next section.

[60] At 2.5 Ga, the lack of methane produces a cooling of 10°C for composition C and 14°C with a mean surface temperature of –2.2°C for composition B (Figure 7).

[61] These results provide new estimates for the composition of Archean atmosphere. If the climate was temperate (mean surface temperature between 10°C and 20°C) and if no other warming process were present, a minimum of 0.1 bar (0.01 bar) of CO_2 with CH_4 at the beginning (the end) of the Archean should have been present in the atmosphere, according to our simulations. Such amounts of CO_2 and CH_4 remain acceptable given the current geological constraints and are consistent with amounts determined by 1-D models [*Haqq-Misra et al.*, 2008; *Kasting and Howard*, 2006]. The presence of methane allows a temperate climate in the absence of haze cooling effect. If methane was present in large quantities (around 2 mbar) at the end of the Archean, the oxidation of the atmosphere in the Early Proterozoic and the destruction of methane would have produced a strong glaciation with a mean surface temperature possibly below the freezing point, but not necessarily a full glaciation (see next section). This scenario could explain the evidence for glaciation in the Early Proterozoic [*Kasting and Ono*, 2006].

[62] To better understand the differences between the present-day climate and the Archean climates, we need to compare simple cases (with no land) with the same mean

Table 2. Global Mean Values for an Aqua-Planet (With Modern Atmospheric Composition and Insolation) and for the Earth at 3.8 Ga With No Land (Atmospheric Composition: 100 Mbar of CO_2 and 2 Mbar of CH_4)

Case	Mean Surface Temperature	Planetary Albedo	Condensed Water	Precipitation
Aqua planet (present Sun)	19°C	0.36	0.19 kg/m^2	4.0e-5 kg/m^2/s
Earth at 3.8 Ga	18.7°C	0.30	0.16 kg/m^2	3.4e-5 kg/m^2/s

surface temperature. Thus, we ran the model for an aqua-planet with the modern atmospheric composition and solar irradiance. This case has approximately the same mean surface temperature as the Earth at 3.8 Ga (still no land) with the atmospheric composition C (see Table 2 and Figure 8). The comparison between the two emphasizes the key characteristics of Archean climates, with reduced Sun and enhanced greenhouse effect.

[63] Our simulations predict a strong decrease in the planetary albedo for the Archean Earth (passing from 0.36 to 0.3 in Table 2). This occurs for two reasons. First, the enhancement of greenhouse gases, in particular methane, increases the shortwave solar radiation absorbed by the atmosphere. Approximately 25% of the incoming solar flux is absorbed by the atmosphere for the Earth at 3.8 Ga with composition C versus 19% for modern Earth. It contributes to approximately half the decrease in the planetary albedo and warms the planet.

[64] Second, the lower solar radiation absorbed by the oceans leads to less clouds. The hydrological cycle is weakened with less evaporation across the planet (see Figure 8). Less clouds are produced (both lower and higher clouds), thereby reducing the planetary albedo. The column mass of clouds is reduced by ∼16% and the cloud cover by ∼10%. This tends to globally warm the planet. Precipitation is also reduced by ∼15%, which would diminish a little the weathering for the Archean Earth.

[65] These differences (warmer poles, a reduced planetary albedo, less clouds and precipitation) are very general and have to appear in any temperate climate of the early Earth.

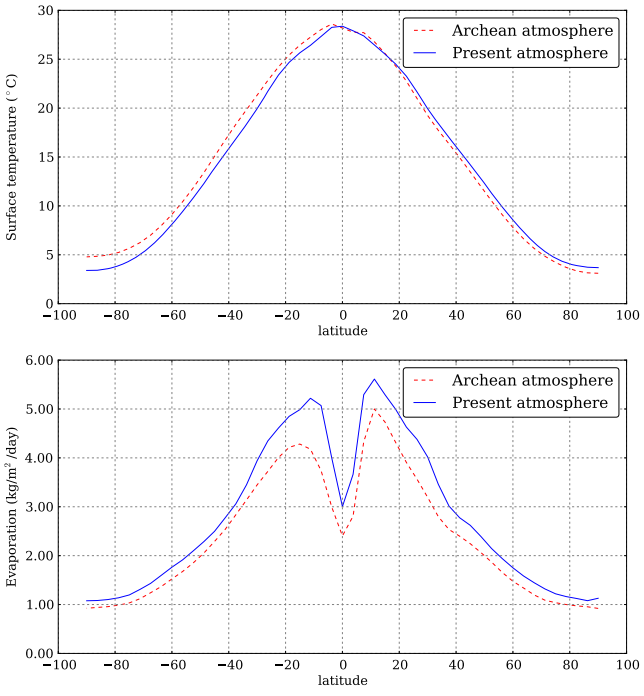

Figure 8. Zonally averaged (top) surface temperature and (bottom) evaporation rate for an aqua planet with present-day atmospheric composition and Sun (solid blue line) and for an aqua planet with 0.1 bar of CO_2, 2 mbar of CH_4, and the Archean Sun at 3.8 Ga (dashed red line).

4.5. Case of a Cold Climate

[66] Here we provide more details on the Archean climates for which the mean surface temperature is below the freezing point. That corresponds to very cold climates with the atmospheric composition B without methane, and composition A with or without methane (Figure 7). According to 1-D models, all these cases should correspond to a full glaciation, while in our simulations, only composition A without methane at 3.8 Ga produces a full snowball Earth. The mean surface temperature can be as low as –25°C keeping an ice-free water belt at the equator (see Figure 9). The sea ice can spread down to 25°N/S without triggering the runaway glaciation. In the coldest case that is not fully frozen (0.9 mbar of CO_2 at 3 Ga), the polar temperatures vary between –45°C and –95°C and the equatorial oceanic temperature is around 6°C.

[67] In our simulations, we notice a decrease of the albedo above the water belt. In a cold climate, the humidity decreases, leading to thinner clouds and hence a lower albedo. This process appears particularly efficient close to the frozen line. The latter corresponds to a cloud-free zone of subsidence. The closer the frozen line goes to the equator, the more the albedo of the tropics decreases. Since this region receives 50% of Earth's solar insolation, a powerful cloud-albedo feedback counteracts the ice-albedo feedback and stops the glaciation. Figure 10 shows the albedo for two cold climates at 3.8 Ga, the first with atmospheric composition A (mean surface temperature = –18°C) and the second with atmospheric composition B (mean surface temperature = 0°C). In the coldest case, the albedo is reduced by 31%

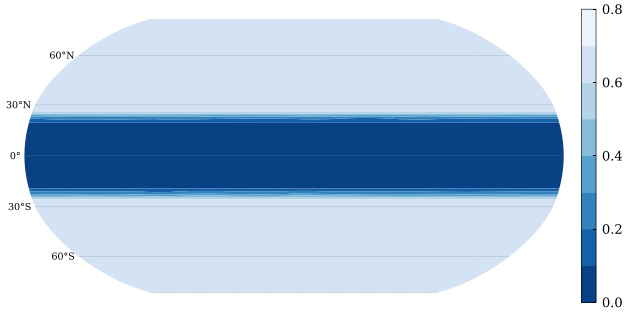

Figure 9. Surface albedo at 3 Ga with no land (atmospheric composition: 0.9 mbar of CO_2 and no CH_4).

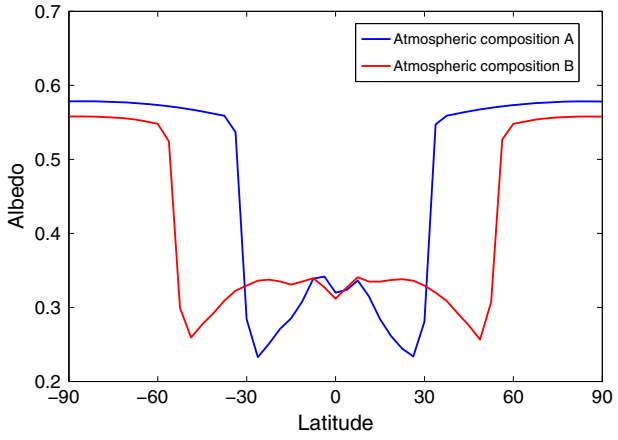

Figure 10. Top of the atmosphere albedo at 3.8 Ga with no land with the atmospheric compositions A (blue) and B (red).

corresponding to additional 30 W/m^2 absorbed by the ocean at 25°N/S, close to the freezing line.

[68] Thus, our model shows that while a full snowball Earth is reached with present-day atmospheric composition (see section 4.1), the Earth appears very resistant to full glaciation if it has a sufficient amount of greenhouse gases (0.9 mbar of CO_2 and CH_4 or even without CH_4 after 3 Ga) thanks to the cloud feedback. Simulations with a coupled climate/ice-sheet model, considering a cloud feedback similar to ours, have also shown that equatorial water belts can be maintained under cold climates providing a solution to the Neoproterozoic glaciations and keeping a refugium for multicellular animals [*Hyde et al.*, 2000].

[69] Our GCM is rather simplified, especially as far as the ocean is concerned. Our oceanic model includes diffusion and Ekman transport for heat but no transport of oceanic ice. *Lewis et al.* [2003] showed that winds, through Ekman transport, could advect sea ice close to the equator helping to trigger the full glaciation. *Kienert et al.* [2012] get the exact opposite result to ours. They found a strong sensitivity of full glaciation to the ice-albedo feedback. In their model, 0.4 bar of CO_2 is required to avoid a full glaciation. This is far larger than with 1-D models or than with our model where 0.9 mbar of CO_2 is sufficient to avoid full glaciation and 0.1 bar of CO_2 yields a warmer climate than today. However, while *Kienert et al.* [2012] use a full oceanic general circulation model, they use a highly simplified atmospheric model with parameterizations of meridional transport. This approach used by these authors does not include cloud feedback effects on their simulated climate.

[70] Thus, studies with other GCMs and in particular GCMs coupled to full oceanic models will be required to estimate more accurately the limit of runaway glaciation for the Archean Earth. But it is still probable that the Earth could have kept water belts with a mean surface temperature below 0°C and with a low amount of greenhouse gases, which mitigates the faint young Sun problem.

5. Additional Warming Processes

[71] In the previous section, we explored conditions for a temperate climate, by changing only the land distribution and the atmospheric composition. However, it appears difficult to reach or exceed the present-day temperatures with the geological constraints on greenhouse gas partial pressure. Other mechanisms such as the microphysics of clouds, the atmospheric pressure, or Earth's rotation rate have been suggested to warm the early Earth. In this section, we study these additional warming processes with our 3-D model.

5.1. Effect of the Cloud Droplet Size

[72] Clouds have a strong impact on the terrestrial radiative budget and a change in their cover or thickness could have had an important effect for the climate of the early Earth [*Goldblatt and Zahnle*, 2011b]. We will focus on the lower clouds, which have a strong impact on the quantity of shortwave radiation arriving on the surface. The removal of all lower clouds compared to the present-day cover would lead to a radiative forcing of 25 W/m^2 [*Goldblatt and Zahnle*, 2011b], i.e., about half of the deficit of radiative forcing due to the weaker Sun during the late Archean. The quantity of cloud condensation nuclei (CCN) is an important factor for cloud microphysics and can control the size of cloud droplets. For the same mass of condensed water, larger amounts of CCN lead to smaller droplets. On the modern Earth, an important fraction of the total amount of CCN comes from biomass burning and human-generated pollution. These anthropic aerosols are more concentrated over land, leading to a smaller cloud droplet radius over land (6–10 μm) than over ocean (10–14 μm) [*Breon et al.*, 2002].

[73] On the prehuman Earth, the quantity of CCNs should have been controlled by biological activity [*Andreae*, 2007], particularly from the dimethylsulfide by algaes and biological particles (including pollen, microbes, and plant debris). Variations of those biological emissions of CCN could have had an impact on the climate, because a reduction of the amount of CCN leads to thinner clouds and so to a lower planetary albedo. That has been suggested to be an explanation of the warm climates of the Cretaceous [*Kump and Pollard*, 2008]. During the Archean, those biological emissions should have been strongly reduced, which should have led to an important warming [*Rosing et al.*, 2010]. *Rosing et al.* [2010] suggested that the cloud droplet radius could have reached 17 μm or larger, leading, for their 1-D model, to a radiative forcing of 22 W/m^2 and a warming of about +10°C. The possibility of reaching such large radii has been debated [*Goldblatt and Zahnle*, 2011a, 2011b] along with the radiative forcing, because of the large uncertainty on the evolution of the precipitation rate with droplet radius.

[74] The visible optical depth of water clouds is given by [*Sanchez-Lavega*, 2011]

$$\tau = \frac{3}{2}\frac{w}{\rho r_e} \tag{13}$$

where w is the column of liquid water (mass per unit area within the cloud), ρ is the volume mass of water, and r_e is the effective radius of the cloud droplets. Thus, larger cloud droplets lead to a lower optical depth in two ways: first, by directly increasing r_e (Twomey effect) [*Twomey*, 1977], and second, by decreasing w due to enhanced precipitation at larger radius (Albrecht effect) [*Albrecht*, 1989]. The first way is very robust while the second is very unclear. Larger droplets should naturally increase precipitation, due to larger cross sections of collisions between droplets yielding a

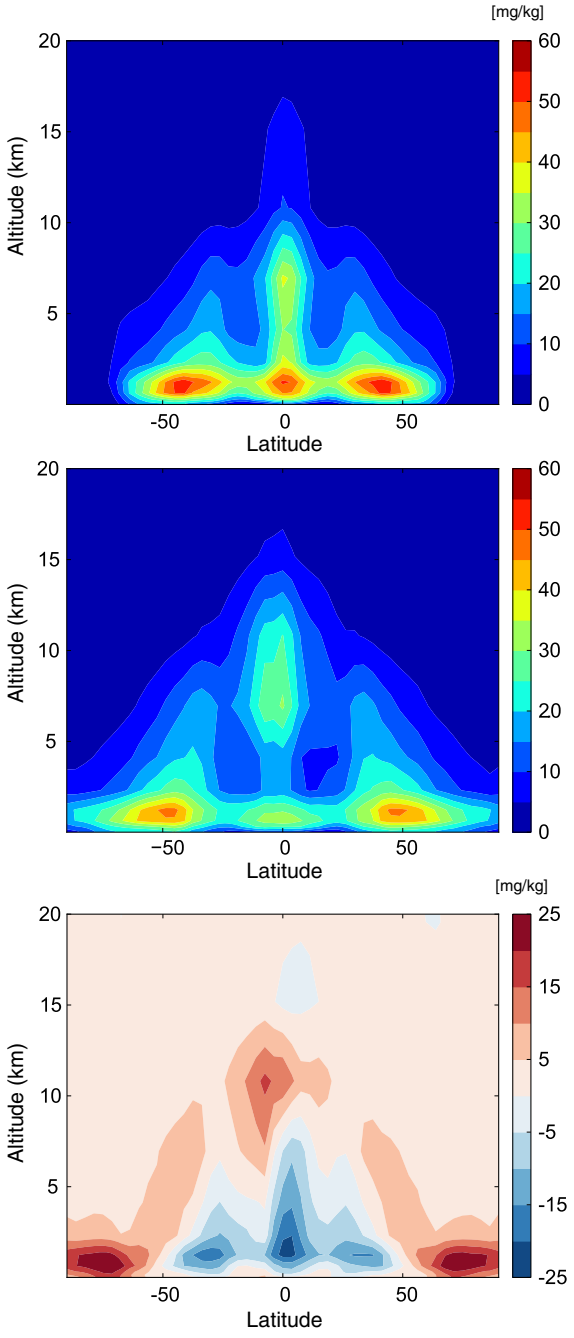

Figure 11. Zonally averaged mixing ratio (in mg/kg of air) of condensed water (liquid and icy clouds) at 2.5 Ga (atmospheric composition: 10 mbar of CO_2 and 2 mbar of CH_4) for liquid droplet radius of (top) 12 μm and (middle) 17 μm. (bottom) The difference between both (17 μm minus 12 μm).

larger autoconversion into raindrops [*Boucher et al.*, 1995]. However, the magnitude of this increase in precipitation is not well known. Moreover, unclear feedbacks could occur, limiting this effect. For instance, precipitation changes the number of CCN locally and hence the radius of droplets. Moreover, a change in clouds impacts surface wind speeds and thus the emission of CCN. Such subtle feedbacks are not taken into account in GCMs, which use fixed radii or fixed amounts of CCN, and simplified parameterizations for rain. This remains an open question.

[75] Parameterizations of enhanced rainout vary from proportional to r/r_0 to proportional to $(r/r_0)^{5.37}$ [*Kump and Pollard*, 2008; *Penner et al.*, 2006; *Goldblatt and Zahnle*, 2011a]. *Kump and Pollard* [2008] and *Rosing et al.* [2010] used an exponent 3, an intermediate value. In our model, we use an exponent 1. This value is in the lower range compared to the literature. However, we believe using a physically based parameterization such as *Boucher et al.* [1995] (see equation (3)) is important to get robust results. That is why we take it as a reference. A comparison using our model with different exponents is given later.

[76] Here we compare simulations with the radius for liquid clouds fixed at 17 μm to simulations with the radius fixed at 12 μm (present-day value used before). Figure 11 shows the mixing ratio of water condensed in the atmosphere (i.e., the mass of cloud per mass of air) at 2.5 Ga with the atmospheric composition B for both radii, and the difference between both. There are less lower clouds (i.e., lower than 5 km) for low and middle latitudes in the case of 17 μm due to the increase in precipitation rate. There are more lower clouds at high latitudes and more higher clouds (i.e., higher than 5 km) at low and middle latitudes. This is due to the warmer surface and to the Hadley cell, which extends deeper in the troposphere. We find a reduction by 10 to 20% of the amount of low- and middle-latitude lower clouds, in agreement with equation (3) to maintain the same precipitation rate. In the tropics (i.e., latitudes between 30°N and 30°S), the mean optical depth of clouds decreases by around 30% (from 37.2 to 26.9). Because of the larger droplets and the lower amount of lower clouds, the net solar absorption increases by 10.3 W/m^2 and the planetary albedo changes from 0.33 to 0.29. The mean surface temperature changes from 11.6°C to 18.8°C with the larger radius, which corresponds to a warming of +7.2°C. Around 4.8°C of warming is due to the direct effect of larger droplets on optical depth (Twomey effect) and around 2.4°C of warming is due to

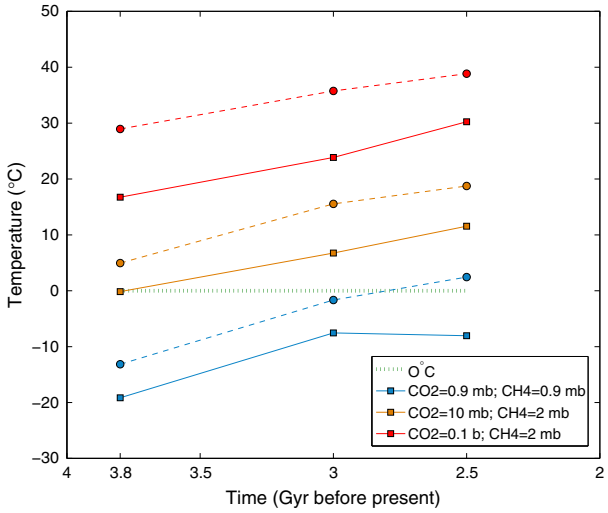

Figure 12. Same as Figure 6 with liquid droplet radius of 12 μm (solid lines with squares) and 17 μm (dashed lines with circles).

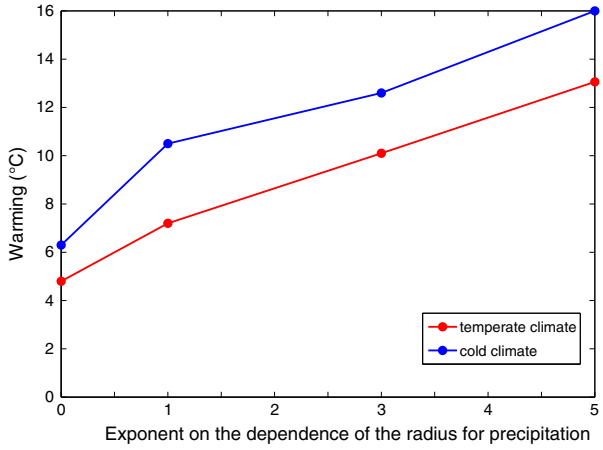

Figure 13. Warming produced by the increase of liquid droplet radius from 12 to 17 μm as a function of the exponent n for the assumption that the precipitation rate is proportional to $(r/r_0)^n$. Simulations at 2.5 Ga with 10 mbar of CO_2 and 2 mbar of CH_4 (red), and 0.9 mbar of $C0_2$ and CH_4 (blue).

the enhanced precipitations (Albrecht effect). We conclude that the first effect is dominant with our model (see next paragraph). Figure 12 presents the mean surface temperature throughout the Archean for our three different atmospheric compositions and with radii of 12 and 17 μm. The warming for every case due to the larger droplets is significant, between +5°C and +12°C.

[77] We now investigate the impact of the change in the exponent on the dependence of radius in the precipitation rate. Figure 13 shows the mean surface temperature for the late Archean with the atmospheric composition B, radius of 17 μm, and the exponent varying from 0 to 5 for cold (atmospheric composition A) and temperate climates (atmospheric composition B). The warming is stronger starting from a cold climate owing to the higher climate sensitivity linked to the ice-albedo feedback under such conditions. Even with no change of the precipitation rate (exponent 0), the warming is significant (between +4.5°C and +6°C). The warming obtained with the exponent 3 (∼ +10°C) is consistent with the model from *Rosing et al.* [2010]. Yet even with the highest exponent, which still remains rather unrealistic, we cannot reach present-day temperatures with the atmospheric composition A. This analysis also reveals that the Twomey effect is dominant for exponents lower than 3, and the Albrecht effect is dominant for exponents higher than 3.

[78] To conclude, larger cloud droplets produce a very efficient warming, even if a large uncertainty remains on the impact of cloud precipitation. That could have helped the Archean Earth to reach a temperate or warm climate but it is not sufficient, according to our model, to solve the faint young Sun problem alone. A significant amount of greenhouse gases is still required. Moreover, the possibility to have droplets reaching 17 μm is still speculative.

5.2. Effect of the Atmospheric Pressure

[79] With the lack of oxygen, the N_2 mixing ratio was probably larger in the Archean than it is presently, making nitrogen the main gas governing atmospheric pressure. Nitrogen is an inert gas with a negligible direct greenhouse effect in terrestrial conditions. However, an increase in atmospheric pressure reinforces the effect of other greenhouse gases through pressure broadening. In the troposphere, the temperature profile is globally often determined by the moist adiabatic lapse rate corresponding to the stability limit of air against moist convection. The moist adiabatic lapse rate given by [*Sanchez-Lavega*, 2011]

$$\Gamma_s = -\left(\frac{\mathrm{d}T}{\mathrm{d}z}\right)_S = \frac{g}{c_p}\left(\frac{1+\frac{L_V x_S}{R_d T}}{1+\frac{L_V^2 x_S}{c_p R_d T^2}}\right) \quad (14)$$

where g is the gravity, c_p is the heat capacity of dry air, L_V is the latent heat of vaporization of water, T is the temperature, R_d and R_v are the gas constants for dry air and water vapor, $x_S = \epsilon \frac{P_{VS}(T)}{P}$ is the saturation mixing ratio where $P_{VS}(T)$ is the saturation vapor pressure, P is the pressure, and $\epsilon = M_w/M_d$ is the ratio of molar masses of water and dry air. An increase in the atmospheric pressure necessarily increases the moist adiabatic lapse rate (going closer to the dry adiabatic lapse rate $\frac{g}{c_p} = -9.8$ K/km). This leads to an additional warming. In return, an increased pressure leads to

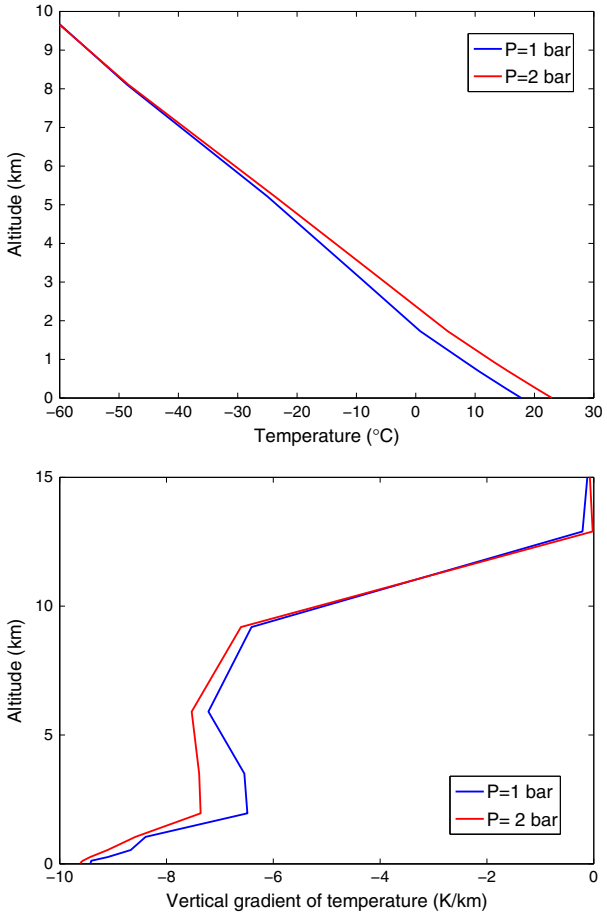

Figure 14. Zonally averaged (top) vertical temperature profiles and (bottom) temperature lapse rate at the equator at 2.5 Ga (atmospheric composition: 10 mbar of CO_2 and 2 mbar of CH_4) with an atmospheric pressure of 1 bar (blue) and 2 bars (red).

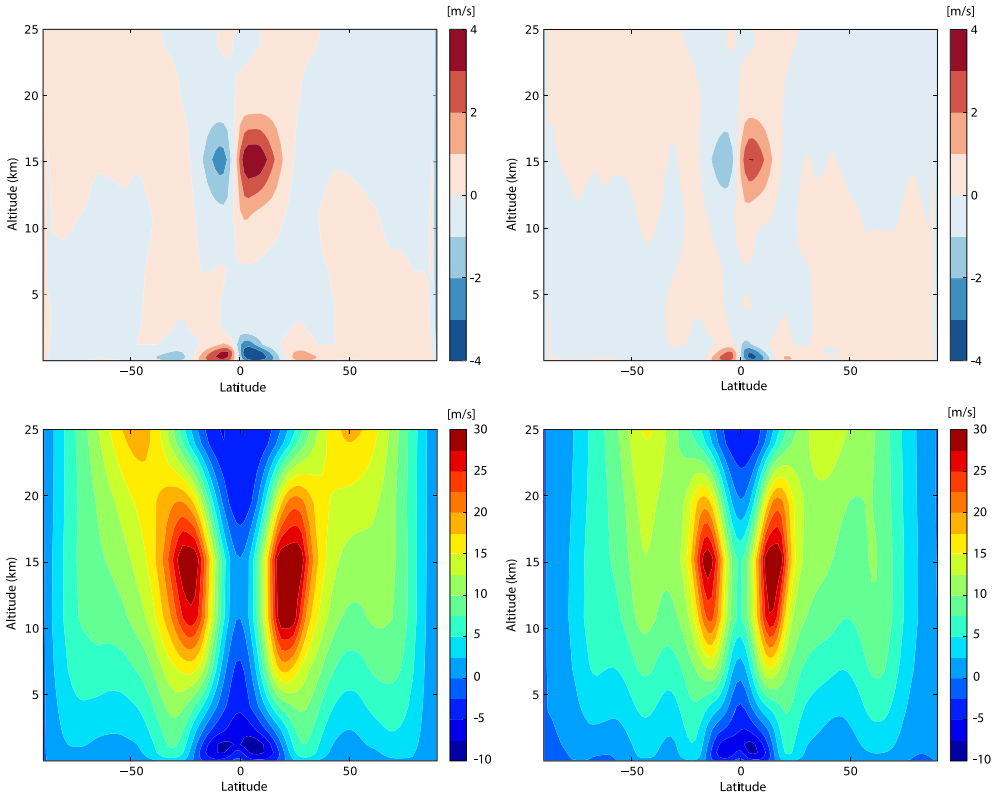

Figure 15. Zonally averaged (top row) meridional and (bottom row) zonal winds for a rotation period of (left column) 24 h or (right column) 14 h. Simulations at 3.8 Ga with 10 mbar of CO_2, 2 mbar of CH_4, and droplet radius of 17 μm.

enhanced Rayleigh scattering by the atmosphere, increasing the planetary albedo, and cooling the surface.

[80] It has been suggested that the pressure was higher in the past [*Goldblatt et al.*, 2009]. The equivalent of about 2 bars of nitrogen is present in the Earth's mantle. That nitrogen was likely initially present in the atmosphere and later fixed by surface organisms and incorporated into the mantle by subduction. This is corroborated by the correlation between N_2 and radiogenic ^{40}Ar contrary to primordial ^{36}Ar in bubbles in oceanic basalt [*Goldblatt et al.*, 2009; *Marty and Dauphas*, 2003]. Nitrogen fixation is biological and would have increased strongly with the appearance of photosynthetic life. That process would have led to a decrease of the amount of nitrogen in the atmosphere [*Goldblatt et al.*, 2009].

[81] Thus, the partial pressure of nitrogen may have reached 2 to 3 bars during the Archean. According to 1-D modeling, a doubling of the present-day atmospheric nitrogen amount could cause a warming of 4–5°C [*Goldblatt et al.*, 2009]. The change in the moist adiabatic lapse rate impacts the formation of convective clouds, and hence the quantity of clouds in the atmosphere. Moreover, a higher atmospheric pressure impacts the transport of heat to poles. Neither is taken into account in 1-D models.

[82] We have run a simulation for the end of the Archean with the atmospheric composition B and 2 bars of nitrogen. Figure 14 illustrates the change in the atmospheric lapse rate. In the troposphere, the temperature lapse rate increases when pressure is doubled. However, we do not notice particular changes in clouds. With the atmospheric composition B, we get a warming of +7°C, which is 2–3°C more than the warming obtained by *Goldblatt et al.* [2009]. The difference is probably related to the higher amount of CH_4 in our simulation (2 mbar versus 0.1 mbar). The accumulated effects of larger droplets and doubling pressure produce a warming of around 10.5°C, less than the sum of both effects taken separately (∼ 14°C).

[83] A higher surface pressure produces an efficient warming of the same magnitude as larger droplets. Yet an analysis of raindrop impact sizes suggests that the air density at 2.7 Ga was close to the modern value and limited to less than twice the modern value [*Som et al.*, 2012]. Thus, the surface pressure was probably close to 0.8–1 bar at the end of the Archean, even if up to 2 bars remain plausible. The pressure may have been higher at older periods, in particular at the beginning of the Archean. Yet recent data of nitrogen isotopes at 3.5 Ga [*Marty et al.*, 2012] do not seem to go that way. This implies questions about when was the nitrogen incorporated into the mantle and by what means.

5.3. Effect of the Rotation Rate

[84] The Moon's tides produce friction which tends to slow down Earth's rotation. By conservation of angular momentum, the Moon tends to move away from Earth [*Williams*, 2000; *Walker and Zahnle*, 1986]. Thus, the Earth was rotating faster in the past. Earth's rotation period is estimated to be around 14 h at 4 Ga [*Zahnle and Walker*, 1987]. A faster rotation rate impacts the climate by reducing the meridional transport [*Stone*, 1972; *Hunt*, 1979; *Kuhn et al.*, 1989; *Feulner*, 2012]. The meridional transport at

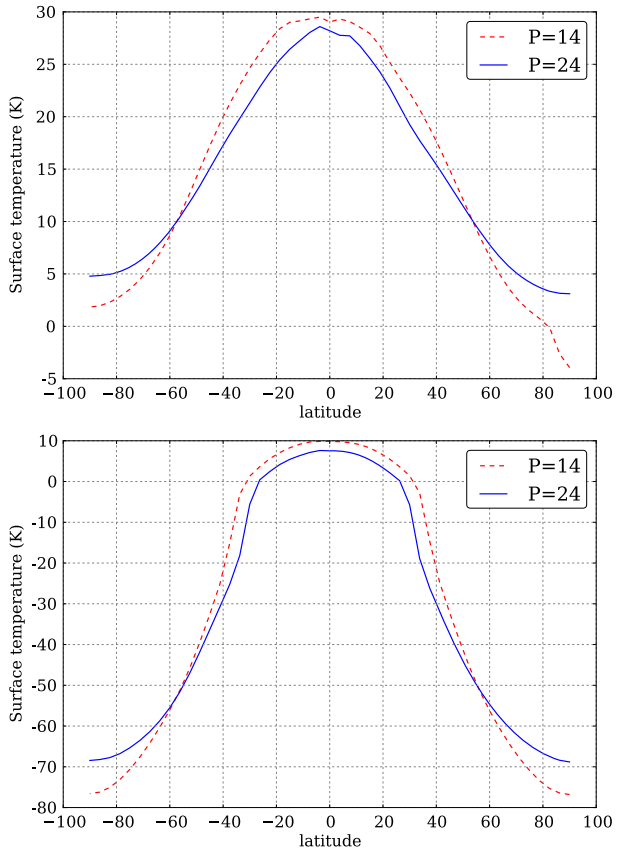

Figure 16. Zonally averaged surface temperature at 3.8 Ga with (top) 100 mbar of CO_2, 2 mbar of CH_4, and (bottom) 0.9 mbar of CO_2 and CH_4. The rotation period is either 14 h (dashed red line) or 24 h (solid blue line).

midlatitudes is mainly produced by baroclinic eddies, whose size is scaled to the Rossby deformation radius L_D, which is linked to the rotation rate Ω by [*Sanchez-Lavega*, 2011]

$$L_D = \frac{N_B H}{f_0} \tag{15}$$

where N_B is the Brunt-Väisälä frequency, H is the scale height, and $f = 2\Omega \sin\phi$ (with ϕ the latitude) is the Coriolis parameter.

[85] A faster rotation rate limits the size of eddies, which decreases the efficiency of meridional transport. Under such conditions, the equator-pole thermal gradient is enhanced with a warmer equator and cooler poles.

[86] We ran the model at 3.8 Ga with a rotation rate of 14 h for different conditions: temperate, warm, and cold climates. For the temperate climate (10 mbar of CO_2, 2 mbar of CH_4, and droplet radius of 17 μm), we found a limited impact of the faster rotation rate. The mean surface temperature in the temperate climate is 1°C lower with the faster rotation rate, and sea ice is more extended, but no significant change in cloud covering and planetary albedo is observed. Figure 15 shows the winds for both rotation rates for the temperate climate. With the faster rotation rate, the latitudinal extension and the strength of the Hadley cells are reduced and the jets are closer to the equator.

[87] In contrast, for a cold and a warm climate (climate with no oceanic ice), a faster rotation rate produces a warming with our model. Figure 16 shows the surface temperature at 3.8 Ga for a warm and a cold climate with a rotation rate of either 24 or 14 h. The mean surface temperature in the warm climate is 1.5°C higher with the faster rotation rate while the mean tropical oceanic temperature is around 2°C higher. Since no ice albedo happens in this case, the mean temperature increases due to the water vapor feedback, which is enhanced in the tropics. In the case of a cold climate, the faster rotation and the reduced meridional transport limit the propagation of sea ice to the equator since the removal of heat from the tropics is less efficient. Water belts are larger (Figure 16) and the triggering of full glaciation is weakened. To summarize, the rotation rate seems to have a very limited impact on the climate of the early Earth. The only notable impact is to make a full glaciation a little bit more difficult.

6. Summary and Discussion

[88] In this paper, we have tested a range of hypotheses to solve the faint young Sun problem and we have obtained new estimates for the greenhouse gases required for a temperate climate for the Archean Earth. We have shown that a CO_2–CH_4-rich atmosphere is a viable solution to the faint young Sun problem. A composition of 10 mbar of CO_2 with 2 mbar of CH_4 allows us to get a temperate climate (mean surface temperature between 10°C and 14°C, which is just a little colder than today) at the end of the Archean while satisfying the geological constraints on the CO_2 partial pressure. At the beginning of the Archean, a partial pressure of around 0.1 bar of CO_2 with 2 mbar of CH_4 is required to get temperate climates if no other warming mechanism occurred. However, no geological constraints for the CO_2 partial pressure at this period currently exist. The presence of only CO_2 would not provide a sufficient greenhouse warming to get temperate climates. The removal of methane at 2.5 Ga produced by the oxidation of the atmosphere in the Early Proterozoic yields a cooling of 14°C. This strong glaciation is not global according to our model. This could be a good scenario for the glaciations of the Early Proterozoic and preserving life in the ice-free water belt.

[89] The Archean Earth most likely featured less emerged land than today. However, a change in land distribution has only a small influence on the ocean temperatures (less than 3°C over the whole Earth and less than 1.5°C over the tropics). The lack of evidence of glaciation during most of the Archean can be interpreted as being caused by a hotter climate than today but also as another distribution of land for a similar or colder climate. An Earth with little emerged land that is essentially concentrated at the equator will only keep geological evidence of full glaciations. The faster rotation of the Archean Earth seems to have a very small impact on the global climate. However, it can limit the triggering of a full snowball Earth a little. Larger cloud droplets appear to be a very efficient way to warm the Archean Earth. The uncertainty in the precipitation rate implies a large uncertainty in the warming, but it remains strong in any case in our simulations (warming between +5°C and +13°C). A better understanding of the different processes and feedbacks implied in precipitation will be required to refine this effect. Moreover, a reduced number of CCN could impact the formation of higher clouds. This could amplify or diminish

Table 3. Effect of the Different Warming Processes for the Earth at 2.5 Ga With 10 Mbar of CO_2 and 2 Mbar of CH_4

Warming Process	Warming
Methane (2 mbar)	+14°C
Less land	≤ +3.5°C
Larger droplet	+7°C
Doubling pressure	+7°C
Larger droplet + doubling pressure	+10.5°C
Faster rotation rate	–1°C

the warming. However, larger droplets during the Archean have yet to be confirmed through geological data, which will be challenging. A higher atmospheric pressure also appears to be an efficient warming process. However, analyses of raindrops imprints [*Som et al.*, 2012] along with recent data [*Marty et al.*, 2012] challenge this process for most of the Archean. These last two hypotheses are not sufficient to solve the faint young Sun problem but they may have played a significant role in complementing the greenhouse effect to CO_2 and CH_4. Table 3 summarizes the different warming processes at 2.5 Ga with 10 mbar of CO_2 with 2 mbar of CH_4.

[90] Our GCM supports some of the main conclusions of 1-D models, but it also reveals some interesting 3-D behavior of the climate. There is a decrease in clouds above continents that compensates for their higher surface albedo and there is especially an important cloud feedback. For the same surface temperature, there are less clouds during the Archean due to the weaker evaporation. This leads to a lower planetary albedo. In our model, another strong cloud feedback appears in cold climates. The decrease of clouds particularly close to the freezing line counteracts the ice-albedo feedback and allows water belts to exist with a mean surface temperature far below the frozen point. Such a resistance against glaciation mitigates the faint young Sun problem.

7. Perspectives

[91] This paper constitutes the first full study of the Archean Earth with a 3-D GCM coupled to a dynamic oceanic model. Coupled 3-D models applied to the early Earth provide new tools for achieving progress in a field where there is still a lot to understand. Three-dimensional GCMs have to be as general (less tuned) as possible. As for global warming, comparison between several GCMs will be required to refine predictions. Our study consolidates many results obtained with 1-D radiative-convective models and emphasizes some particular behaviors inherent to 3-D as well. There are many ways to solve the faint young Sun problem. According to our results, it is not so difficult a task, particularly if cold climates with water belts can be maintained. New geological constraints for the early Archean on CO_2 and N_2 partial pressures, as well as the H_2 abundance of the atmosphere, are necessary to have a good picture of the atmospheric composition.

[92] There are many perspectives for future research with our new modeling tool. First, the levels of CH_4 we used could lead to the formation of organic haze, in particular for the end of the Archean, where some geological data could be interpreted as the episodic formation of haze [*Zerkle et al.*, 2012]. The study of the formation, dynamics, and anti-greenhouse effect of organic haze with a 3-D model would constitute major progress on this topic. Finally, although it appears possible to get a temperate climate during the Archean, producing a hot early Earth with oceans at 60°C to 80°C, as suggested from oceanic cherts [*Robert and Chaussidon*, 2006], requires a far stronger warming. Although this idea is controversial, it would be interesting to see what pressure of CO_2, in addition to other warming processes (higher pressure, larger cloud droplets, methane) would be required more precisely than with 1-D models. Such a study would also be applicable to the Hadean Earth.

[93] **Acknowledgments.** We thank Olivier Boucher for discussions of cloud formation and precipitations.

References

Abbot, D. S., A. Voigt, and D. Koll (2011), The Jormungand global climate state and implications for Neoproterozoic glaciations, *J. Geophys. Res.*, *116*, D18103, doi:10.1029/2011JD015927.

Albrecht, B. A. (1989), Aerosols, cloud microphysics, and fractional cloudiness, *Science*, *245*, 1227–1230, doi:10.1126/science.245.4923.1227.

Andreae, M. O. (2007), Aerosols before pollution, *Science*, *315*(5808), 50–51, doi:10.1126/science.1136529.

Battistuzzi, F. U., A. Feijao, and S. B. Hedges (2004), A genomic timescale of prokaryote evolution: Insights into the origin of methanogenesis, phototrophy, and the colonization of land, *BMC Evol. Biol.*, *4*(1), 44, doi:10.1186/1471-2148-4-44.

Belousova, E. A., Y. A. Kostitsyn, W. L. Griffin, G. C. Begg, S. Y. O'Reilly, and N. J. Pearson (2010), The growth of the continental crust: Constraints from zircon Hf-isotope data, *Lithos*, *119*, 457–466, doi:10.1016/j.lithos.2010.07.024.

Blake, R. E., S. J. Chang, and A. Lepland (2010), Phosphate oxygen isotopic evidence for a temperate and biologically active Archaean ocean, *Nature*, *464*, 1029–1032, doi:10.1038/nature08952.

Boucher, O., H. Le Treut, and M. B. Baker (1995), Precipitation and radiation modeling in a general circulation model: Introduction of cloud microphysical processes, *J. Geophys. Res.*, *100*, 16,395–16,414, doi:10.1029/95JD01382.

Bousseau, B., S. Blanquart, A. Necsulea, N. Lartillot, and G. Manolo (2008), Parallel adaptations to high temperatures in the Archaean eon, *Nature*, *456*, 942–945, doi:10.1038/nature07393.

Breon, F. M., D. Tanré, and S. Generoso (2002), Aerosol effect on cloud droplet size monitored from satellite, *Science*, *295*, 834–838, doi:10.1126/science.1066434.

Charnay, B., and S. Lebonnois (2012), Two boundary layers in Titan's lower troposphere inferred from a climate model, *Nat. Geosci.*, *5*, 106–109.

Clough, S. A., M. J. Iacono, and J.-L. Moncet (1992), Line-by-line calculations of atmospheric fluxes and cooling rates: Application to water vapor, *J. Geophys. Res.*, *97*(15), 15,761–15,785, doi:10.1029/92JD01419.

Codron, F. (2012), Ekman heat transport for slab oceans, *Clim. Dyn.*, *38*, 379–389.

Dhuime, B., C. J. Hawkesworth, P. A. Cawood, and C. D. Storey (2012), A change in the geodynamics of continental growth 3 billion years ago, *Science*, *335*, 1334–1336, doi:10.1126/science.1216066.

Domagal-Goldman, S. D., J. F. Kasting, D. T. Johnston, and J. Farquhar (2008), Organic haze, glaciations and multiple sulfur isotopes in the mid-Archean era, *Earth Planet. Sci. Lett.*, *269*, 29–40, doi:10.1016/j.epsl.2008.01.040.

Driese, S. G., M. A. Jirsa, M. Ren, S. L. Brantley, N. D. Sheldon, D. Parker, and M. Schmitz (2011), Neoarchean paleoweathering of tonalite and metabasalt: Implications for reconstructions of 2.69 Ga early terrestrial ecosystems and paleoatmospheric chemistry, *Precambrian Res.*, *189*, 1–17, doi:10.1016/j.precamres.2011.04.003.

Evans, D. A., N. J. Beukes, and J. L. Kirschvink (1997), Low-latitude glaciation in the Palaeoproterozoic era, *Nature*, *386*, 262–266, doi:10.1038/386262a0.

Feulner, G. (2012), The faint young Sun problem, *Rev. Geophys.*, *50*, RG2006, doi:10.1029/2011RG000375.

Flament, N., N. Coltice, and P. F. Rey (2008), A case for late-Archaean continental emergence from thermal evolution models and hypsometry, *Earth Planet. Sci. Lett.*, *275*, 326–336, doi:10.1016/j.epsl.2008.08.029.

Forget, F., F. Hourdin, R. Fournier, C. Hourdin, O. Talagrand, M. Collins, S. R. Lewis, P. L. Read, and J.-P. Huot (1999), Improved general circulation models of the Martian atmosphere from the surface to above 80 km, *J. Geophys. Res.*, *104*, 24,155–24,176.

Forget, F., F. Hourdin, R. Fournier, C. Hourdin, O. Talagrand, M. Collins, S. R. Lewis, P. L. Read, and J.-P. Huot (2012), Global modelling of the early Martian climate under a denser CO_2 atmosphere: Temperature and CO_2 ice clouds, *Icarus*, *104*, 24,155–24,176.

Francois, L. M., and J.-C. Gerard (1988), Ozone, climate and biospheric environment in the ancient oxygen-poor atmosphere, *Planet. Space Sci.*, *36*, 1391–1414, doi:10.1016/0032-0633(88)90007-4.

Frierson, D. M. W. (2007), The dynamics of idealized convection schemes and their effect on the zonally averaged tropical circulation, *J. Atmos. Sci.*, *64*, 1959–1976.

Gaillard, F., B. Scaillet, and N. T. Arndt (2011), Atmospheric oxygenation caused by a change in volcanic degassing pressure, *Nature*, *478*(7368), 229–232, doi:10.1038/nature10460.

Gaucher, E. A., S. Govindarajan, and O. K. Ganesh (2008), Palaeotemperature trend for Precambrian life inferred from resurrected proteins, *Nature*, *452*, 704–707, doi:10.1038/nature06510.

Goldblatt, C., and K. J. Zahnle (2011a), Faint young Sun paradox remains, *Nature*, *474*, 744–747, doi:10.1038/nature09961.

Goldblatt, C., and K. J. Zahnle (2011b), Clouds and the faint young Sun paradox, *Clim. Past*, *7*, 203–220, doi:10.5194/cp-7-203-2011.

Goldblatt, C., M. W. Claire, T. M. Lenton, A. J. Matthews, A. J. Watson, and K. J. Zahnle (2009), Nitrogen-enhanced greenhouse warming on early Earth, *Nat. Geosci.*, *2*, 891–896, doi:10.1038/ngeo692.

Gough, D. O. (1981), Solar interior structure and luminosity variations, *Sol. Phys.*, *74*, 21–34, doi:10.1007/BF00151270.

Gregory, D. (1995), A consistent treatment of the evaporation of rain and snow for use in large-scale models, *Mon. Weather Rev.*, *123*, 2716–2732, doi:10.1175/1520-0493(1995)123<2716:ACTOTE>2.0.CO;2.

Hansen, J. E., and L. D. Travis (1974), Light scattering in planetary atmospheres, *Space Sci. Rev.*, *16*, 527–610, doi:10.1007/BF00168069.

Haqq-Misra, J. D., S. D. Domagal-Goldman, P. J. Kasting, and J. F. Kasting (2008), A revised, hazy methane greenhouse for the Archean Earth, *Astrobiology*, *8*, 1127–1137, doi:10.1089/ast.2007.0197.

Hessler, A. M., D. R. Lowe, R. L. Jones, and D. K. Bird (2004), A lower limit for atmospheric carbon dioxide levels 3.2 billion years ago, *Nature*, *428*, 736–738, doi:10.1038/nature02471.

Hourdin, F., et al. (2006), The LMDZ4 general circulation model: Climate performance and sensitivity to parametrized physics with emphasis on tropical convection, *Clim. Dyn.*, *27*, 787–813.

House, C. H., B. Runnegar, and S. T. Fitz-Gibbon (2003), Geobiological analysis using whole genome-based tree building applied to the bacteria, archaea, and eukarya, *Geobiology*, *1*(1), 15–26, doi:10.1046/j.1472-4669.2003.00004.x.

Hren, M. T., M. M. Tice, and C. P. Chamberlain (2009), Oxygen and hydrogen isotope evidence for a temperate climate 3.42 billion years ago, *Nature*, *462*, 205–208, doi:10.1038/nature08518.

Hunt, B. G (1979), The effects of past variations of the Earth's rotation rate on climate, *Nature*, *281*(5728), 188–191, doi:10.1038/281188a0.

Hyde, W. T., T. J. Crowley, S. K. Baum, and W. R. Peltier (2000), Neoproterozoic "snowball Earth" simulations with a coupled climate/ice-sheet model, *Nature*, *405*, 425–429.

Jaffrés, J. B. D., G. A. Shields, and K. Wallmann (2007), The oxygen isotope evolution of seawater: A critical review of a long-standing controversy and an improved geological water cycle model for the past 3.4 billion years, *Earth Sci. Rev.*, *83*, 83–122, doi:10.1016/j.earscirev.2007.04.002.

Jenkins, G. (1999), Examining the sensitivity of Earth's climate to the removal of ozone, land masses and enhanced ocean heat transport in the GENESIS global climate model, *Global Planet. Change*, *20*, 257–279.

Jenkins, G. S. (1993), A general circulation model study of the effects of faster rotation rate, enhanced CO_2 concentration, and reduced solar forcing: Implications for the faint young Sun paradox, *J. Geophys. Res.*, *98*, 20,803–20,811.

Jenkins, G. S. (1995), Early Earth's climate: Cloud feedback from reduced land fraction and ozone concentrations, *Geophys. Res. Lett.*, *22*, 1513–1516.

Jenkins, G. S., H. G. Marshall, and W. R. Kuhn (1993), Precambrian climate: The effects of land area and Earth's rotation rate, *J. Geophys. Res.*, *98*, 8785–8791.

Kasting, J. F., and T. P. Ackerman (1986), Climatic consequences of very high carbon dioxide levels in the Earth's early atmosphere, *Science*, *234*, 1383–1385, doi:10.1126/science.234.4782.1383.

Kasting, J. F., and T. M. Howard (2006), Atmospheric composition and climate on the early Earth, *Philos. Trans. R. Soc.*, *361*, 1733–1742, doi:10.1098/rstb.2006.1902.

Kasting, J. F., and S. Ono (2006), Palaeoclimates: The first two billion years, *Philos. Trans. R. Soc.*, *361*, 917–929, doi:10.1098/rstb.2006.1839.

Kasting, J. F., J. B. Pollack, and D. Crisp (1984), Effects of high CO_2 levels on surface temperature and atmospheric oxidation state of the early Earth, *J. Atmos. Chem.*, *1*, 403–428.

Kasting, J. F., M. T. Howard, K. Wallmann, J. Veizer, G. Shields, and J. Jaffres (2006), Paleoclimates, ocean depth, and the oxygen isotopic composition of seawater, *Earth Planet. Sci. Lett.*, *252*, 82–93, doi:10.1016/j.epsl.2006.09.029.

Kelley, D. S., et al. (2005), A serpentinite-hosted ecosystem: The Lost City hydrothermal field, *Science*, *307*, 1428–1434, doi:10.1126/science.1102556.

Kharecha, P., J. Kasting, and J. Siefert (2005), A coupled atmosphere ecosystem model of the early Archean Earth, *Geobiology*, *3*(2), 53–76, doi:10.1111/j.1472-4669.2005.00049.x.

Kiehl, J. T., and B. A. Boville (1988), The radiative-dynamical response of a stratospheric-tropospheric general circulation model to changes in ozone, *J. Atmos. Sci.*, *45*, 1798–1817, doi:10.1175/1520-0469(1988)045<1798:TRDROA>2.0.CO;2.

Kiehl, J. T., and R. E. Dickinson (1987), A study of the radiative effects of enhanced atmospheric CO_2 and CH_4 on early Earth surface temperatures, *J. Geophys. Res.*, *92*, 2991–2998, doi:10.1029/JD092iD03p02991.

Kienert, H., G. Feulner, and V. Petoukhov (2012), Faint young Sun problem more severe due to ice-albedo feedback and higher rotation rate of the early Earth, *Geophys. Res. Lett.*, *39*, L23710, doi:10.1029/2012GL054381.

Knauth, L. P., and D. R. Lowe (2003), High Archean climatic temperature inferred from oxygen isotope geochemistry of cherts in the 3.5 Ga Swaziland supergroup, South Africa, *Geol. Soc. Am. Bull.*, *115*, 566–580, doi:10.1130/0016-7606(2003)115<0566:HACTIF>2.0.CO;2.

Kuhn, W. R., and S. K. Atreya (1979), Ammonia photolysis and the greenhouse effect in the primordial atmosphere of the Earth, *Icarus*, *37*, 207–213, doi:10.1016/0019-1035(79)90126-X.

Kuhn, W. R., J. C. G. Walker, and H. G. Marshall (1989), The effect on Earth's surface temperature from variations in rotation rate, continent formation, solar luminosity, and carbon dioxide, *J. Geophys. Res.*, *94*, 11,129–11,136, doi:10.1029/JD094iD08p11129.

Kump, L. R., and M. Barley (2008), Increased subaerial volcanism and the rise of atmospheric oxygen 2.5 billion years ago, *Nature*, *448*, 1033–1036, doi:10.1038/nature06058.

Kump, L. R., and D. Pollard (2008), Amplification of Cretaceous warmth by biological cloud feedbacks, *Science*, *320*, 195, doi:10.1126/science.1153883.

Langleben, M. P. (1954), The terminal velocity of snowflakes, *Q. J. R. Meteorolog. Soc.*, *80*, 174–181.

Le Treut, H., and Z. X. Li (1991), Sensitivity of an atmospheric general circulation model to prescribed SST changes: Feedback effects associated with the simulation of cloud optical properties, *Clim. Dyn.*, *5*, 175–187.

Lebonnois, S., F. Hourdin, V. Eymet, A. Crespin, R. Fournier, and F. Forget (2010), Superrotation of Venus' atmosphere analyzed with a full general circulation model, *J. Geophys. Res.*, *115*, E06006, doi:10.1029/2009JE003458.

Lebonnois, S., J. Burgalat, P. Rannou, and B. Charnay (2012), Titan global climate model: A new 3-dimensional version of the IPSL Titan GCM, *Icarus*, *218*, 707–722, doi:10.1016/j.icarus.2011.11.032.

Leconte, J., F. Forget, B. Charnay, R. Wordsworth, F. Selsis, and E. Millour (2013), 3D climate modeling of close-in land planets: Circulation patterns, climate moist bistability and habitability, *Astron. Astrophys.*, doi:10.1051/0004-6361/201321042.

Lewis, J. P., A. J. Weaver, S. T. Johnston, and M. Eby (2003), Neoproterozoic "snowball Earth": Dynamic sea ice over a quiescent ocean, *Paleoceanography*, *18*, 1092, doi:10.1029/2003PA000926.

Lin, B., B. A. Wielicki, L. H. Chambers, Y. Hu, and K.-M. Xu (2002), The iris hypothesis: A negative or positive cloud feedback?, *J. Clim.*, *15*, 3–7, doi:10.1175/1520-0442(2002)015<0003:TIHANO>2.0.CO;2.

Lindzen, R. S., M.-D. Chou, and A. Y. Hou (2001), Does the Earth have an adaptive infrared iris?, *Bull. Am. Meteorol. Soc.*, *82*, 417–432, doi:10.1175/1520-0477(2001)082<0417:DTEHAA>2.3.CO;2.

Manabe, S., and R. T. Wetherald (1967), Thermal equilibrium of the atmosphere with a given distribution of relative humidity, *J. Atmos. Sci.*, *24*, 241–259.

Marshall, J., D. Ferreira, J.-M. Campin, and D. Enderton (2007), Mean climate and variability of the atmosphere and ocean on an aquaplanet, *J. Atmos. Sci.*, *64*, 4270, doi:10.1175/2007JAS2226.1.

Marty, B., and N. Dauphas (2003), The nitrogen record of crust-mantle interaction and mantle convection from Archean to present, *Earth Planet. Sci. Lett.*, *206*, 397–410, doi:10.1016/S0012-821X(02)01108-1.

Marty, B., L. Zimmermann, R. Burgess, M. Pujol, and P. Philippo (2012), Nitrogen partial pressure in the Archean atmosphere from analysis of

hydrothermal quartz, Abstract V54B-04 presented at 2012 Fall Meeting, AGU, San Francisco, Calif.

McKay, C. P., J. B. Pollack, and R. Courtin (1991), The greenhouse and antigreenhouse effects on Titan, *Science*, *253*, 1118–1121, doi:10.1126/science.253.5024.1118.

Mellor, G. L., and T. Yamada (1982), Development of a turbulence closure model for geophysical fluid problems, *Rev. Geophys. Space Phys.*, *20*, 851–875.

Mojzsis, S. J., G. Arrhenius, K. D. McKeegan, T. M. Harrison, A. P. Nutman, and C. R. L. Friend (1996), Evidence for life on Earth before 3,800 million years ago, *Nature*, *384*, 55–59, doi:10.1038/384055a0.

Nisbet, E. G., and N. H. Sleep (2001), The habitat and nature of early life, *Nature*, *409*, 1083–1091.

Owen, T., R. D. Cess, and V. Ramanathan (1979), Enhanced CO_2 greenhouse to compensate for reduced solar luminosity on early Earth, *Nature*, *277*, 640–642, doi:10.1038/277640a0.

Pavlov, A. A., J. F. Kasting, L. L. Brown, K. A. Rages, and R. Freedman (2000), Greenhouse warming by CH_4 in the atmosphere of early Earth, *J. Geophys. Res.*, *105*, 11,981–11,990, doi:10.1029/1999JE001134.

Penner, J. E., J. Quaas, T. Storelvmo, T. Takemura, O. Boucher, H. Guo, A. Kirkevag, J. E. Kristjansson, and Ø. Seland (2006), Model intercomparison of indirect aerosol effects, *Atmos. Chem. Phys.*, *6*, 3391–3405.

Perrin, M. Y., and J. M. Hartmann (1989), Temperature-dependent measurements and modeling of absorption by CO2-N2 mixtures in the far line-wings of the 4.3-micron CO_2 band, *J. Quant. Spectrosc. Radiat. Transfer*, *42*, 311–317, doi:10.1016/0022-4073(89)90077-0.

Pope, E. C., D. K. Bird, and M. T. Rosing (2012), Isotope composition and volume of Earth's early oceans, *PNAS*, *109*(12), 4371–4376, doi:10.1073/pnas.1115705109.

Reinhard, C., and N. Planavsky (2011), Mineralogical constraints on Precambrian pCO_2, *Nature*, *474*, doi:10.1038/nature09959.

Robert, F., and M. Chaussidon (2006), A palaeotemperature curve for the precambrian oceans based on silicon isotopes in cherts, *Nature*, *443*, 969–972, doi:10.1038/nature05239.

Rondanelli, R., and R. S. Lindzen (2010), Can thin cirrus clouds in the tropics provide a solution to the faint young Sun paradox?, *J. Geophys. Res.*, *115*, D02108, doi:10.1029/2009JD012050.

Rosing, M. T. (1999), 13C-depleted carbon microparticles in >3700-Ma sea-floor sedimentary rocks from west greenland, *Science*, *283*, 674–676, doi:10.1126/science.283.5402.674.

Rosing, M. T., D. K. Bird, N. H. Sleep, and C. J. Bjerrum (2010), No climate paradox under the faint early Sun, *Nature*, *464*, 744–747, doi:10.1038/nature08955.

Rothman, L. S., et al. (2009), The HITRAN 2008 molecular spectroscopic database, *J. Quant. Spectrosc. Radiat. Transfer*, *110*, 533–572, doi:10.1016/j.jqsrt.2009.02.013.

Rye, R., P. H. Kuo, and H. D. Holland (1995), Atmospheric carbon dioxide concentrations before 2.2 billion years ago, *Nature*, *378*, 603–605, doi:10.1038/378603a0.

Sagan, C., and G. Mullen (1972), Earth and Mars: Evolution of atmospheres and surface temperatures, *Science*, *177*, 52–56, doi:10.1126/science.177.4043.52.

Sanchez-Lavega, A. (2011), *An Introduction to Planetary Atmosphere*, CRC Press, New York.

Schopf, J. W. (2006), Fossil evidence of Archaean life, *Philos. Trans. R. Soc.*, *361*, 869–855, doi:10.1098/rstb.2006.1834.

Sekhon, R. S., and R. C. Srivastava (1970), Snow size spectra and radar reflectivity, *J. Atmos. Sci.*, *27*, 299–307.

Sheldon, N. (2006), Precambrian paleosols and atmospheric CO_2 levels, *Precambrian Res.*, *147*, 148–155, doi:10.1016/j.precamres.2006.02.004.

Sleep, N. H., and K. Zahnle (2001), Carbon dioxide cycling and implications for climate on ancient Earth, *J. Geophys. Res.*, *106*, 1373–1400, doi:10.1029/2000JE001247.

Som, S. M., D. C. Catling, J. P. Harnmeijer, P. M. Polivka, and R. Buick (2012), Air density 2.7 billion years ago limited to less than twice modern levels by fossil raindrop imprints, *Nature*, *484*(7394), 359–362, doi:10.1038/nature10890.

Stone, P. H. (1972), A simplified radiative-dynamical model for the static stability of rotating atmospheres, *J. Atmos. Sci.*, *29*, 405–418, doi:10.1175/1520-0469(1972)029<0405:ASRDMF>2.0.CO;2.

Tian, F., O. B. Toon, A. A. Pavlov, and H. De Sterck (2005), A hydrogen-rich early Earth atmosphere, *Science*, *308*, 1014–1017, doi:10.1126/science.1106983.

Tian, F., J. F. Kasting, and K. Zahnle (2011), Revisiting HCN formation in Earth's early atmosphere, *Earth Planet. Sci. Lett.*, *308*, 417–423, doi:10.1016/j.epsl.2011.06.011.

Toon, O. B., C. P. McKay, T. P. Ackerman, and K. Santhanam (1989), Rapid calculation of radiative heating rates and photodissociation rates in inhomogeneous multiple scattering atmospheres, *J. Geophys. Res.*, *94*, 16,287–16,301, doi:10.1029/JD094iD13p16287.

Trainer, M. G., A. A. Pavlov, H. L. Dewitt, J. L. Jimenez, C. P. McKay, O. B. Toon, and M. A. Tolbert (2006), Organic haze on Titan and the early Earth, *PNAS*, *103*, 18,035–18,042, doi:10.1073/pnas.0608561103.

Twomey, S. (1977), The influence of pollution on the shortwave albedo of clouds, *J. Atmos. Sci.*, *34*, 1149–1154, doi:10.1175/1520-0469(1977)034<1149:TIOPOT>2.0.CO;2.

van den Boorn, S., M. van Bergen, W. Nijman, and P. Vroon (2007), Dual role of seawater and hydrothermal fluids in early Archean chert formation: Evidence from silicon isotopes, *Geology*, *35*, 939–942, doi:10.1130/G24096A.1.

von Paris, P., H. Rauer, J. Lee Grenfell, B. Patzer, P. Hedelt, B. Stracke, T. Trautmann, and F. Schreier (2008), Warming the early Earth-CO_2 reconsidered, *Planet. Space Sci.*, *56*, 1244–1259, doi:10.1016/j.pss.2008.04.008.

Walker, J. C. G. (1985), Carbon dioxide on the early Earth, *Origins Life Evol. Biosphere*, *16*, 117–127, doi:10.1007/BF01809466.

Walker, J. C. G., and K. J. Zahnle (1986), Lunar nodal tide and distance to the moon during the precambrian, *Nature*, *320*, 600–602, doi:10.1038/320600a0.

Walker, J. C. G., P. B. Hays, and J. F. Kasting (1981), A negative feedback mechanism for the long-term stabilization of the Earth's surface temperature, *J. Geophys. Res.*, *86*, 9776–9782, doi:10.1029/JC086iC10p09776.

Williams, G. E. (2000), Geological constraints on the precambrian history of Earth's rotation and the moon's orbit, *Rev. Geophys.*, *38*, 37–60, doi:10.1029/1999RG900016.

Wolf, E. T., and O. B. Toon (2010), Fractal organic hazes provided an ultraviolet shield for early Earth, *Science*, *328*, 1266–1268, doi:10.1126/science.1183260.

Wordsworth, R., and R. Pierrehumbert (2013), Hydrogen-nitrogen greenhouse warming in Earth's early atmosphere, *Science*, *339*, 64–67, doi:10.1126/science.1225759.

Wordsworth, R., F. Forget, and V. Eymet (2010), Infrared collision-induced and far-line absorption in dense CO_2 atmospheres, *Icarus*, *210*, 992–997, doi:10.1016/j.icarus.2010.06.010.

Wordsworth, R., F. Forget, E. Millour, J. Head, J.-B. Madeleine, and B. Charnay (2012), Global modelling of the early martian climate under a denser CO_2 atmosphere: Water cycle and ice evolution, *Icarus*, *222*, 1–19.

Wordsworth, R. D., F. Forget, F. Selsis, E. Millour, B. Charnay, and J.-B. Madeleine (2011), Gliese 581d is the first discovered terrestrial-mass exoplanet in the habitable zone, *Astrophys. J. Lett.*, *733*, L48.

Young, G. M., V. V. Brunn, D. J. C. Gold, and W. E. L. Minter (1998), Earth'S oldest reported glaciation: Physical and chemical evidence from the Archean Mozaan Group (2.9 Ga) of South Africa, *J. Geol.*, *106*, 523–538, doi:10.1086/516039.

Zahnle, K., and J. C. G. Walker (1987), A constant daylength during the Precambrian era?, *Precambrian Res.*, *37*, 95–105.

Zahnle, K. J. (1986), Photochemistry of methane and the formation of hydrocyanic acid (HCN)in the Earth's early atmosphere, *J. Geophys. Res.*, *91*, 2819–2834, doi:10.1029/JD091iD02p02819.

Zerkle, A. L., M. W. Claire, S. D. Domagal-Goldman, J. Farquhar, and S. W. Poulton (2012), A bistable organic-rich atmosphere on the Neoarchaean Earth, *Nat. Geosci.*, *5*, 359–363, doi:10.1038/ngeo1425.